creative commons
COMMONS DEED

저작자표시-비영리-변경금지 2.0 대한민국

이용자는 아래의 조건을 따르는 경우에 한하여 자유롭게

- 이 저작물을 복제, 배포, 전송, 전시, 공연 및 방송할 수 있습니다.

다음과 같은 조건을 따라야 합니다:

저작자표시. 귀하는 원저작자를 표시하여야 합니다.

비영리. 귀하는 이 저작물을 영리 목적으로 이용할 수 없습니다.

변경금지. 귀하는 이 저작물을 개작, 변형 또는 가공할 수 없습니다.

- 귀하는, 이 저작물의 재이용이나 배포의 경우, 이 저작물에 적용된 이용허락조건을 명확하게 나타내어야 합니다.
- 저작권자로부터 별도의 허가를 받으면 이러한 조건들은 적용되지 않습니다.

저작권법에 따른 이용자의 권리는 위의 내용에 의하여 영향을 받지 않습니다.

이것은 이용허락규약(Legal Code)을 이해하기 쉽게 요약한 것입니다.

Disclaimer

dCollection

공학석사학위논문

고체추진기관 FSI 해석을 위한 2 차원 3 차원 비정렬 점성 격자 자동 재생성 프로그램 개발

Development of Two- and Three-Dimensional Unstructured Viscous Grid Regeneration Technique for Solid Rocket FSI analysis

2018 년 8 월

서울대학교 대학원

기계항공공학부

김 종 인

Abstract

Development of a Two- and Three-Dimensional Unstructured Viscous Grid Regeneration Technique for Solid Rocket FSI Analysis

Jongin Kim

Mechanical and Aerospace Engineering

The Graduate School

Seoul National University

The inside of the solid-propellant rocket motor has many difficulties for the numerical analysis because of the combustion of the propellant, the high temperature and high pressure flow and the structural deformation of the propellant. It involves complex physical phenomena which are influenced by each domain.

The analytical region of the solid-propellant rocket motor is divided into the fluid region, the structure region and the combustion region. The deformation occurs in each region over time. Therefore, it is necessary to generate a suitable grid for the analytical domain that deforms over time. In addition, it is necessary to generate suitable grids for the boundary layer for efficient and accurate viscous flow analysis.

When the grid deformation is periodical such as the aero-elastic analysis, the grid-moving

method and the grid deformation method are used. On the other hand, because the solid-propellant rocket motor is a variation of the area due to the continuous combustion, unlike the above-mentioned problem, it is difficult to generate the grid by the two techniques. Therefore, it is necessary to regenerate the entire grid automatically during the analysis, which is called the ‘grid regeneration technique’. It is important that the grid regeneration technique usually has a stable and efficient grid generation process without user intervention.

In the case of internal flow geometries such as solid propulsion rocket engines, unlike ordinary external flow geometries, overlap between neighborhood grids occurs during the automatic grid generation process, and inevitably invalid grids can be generated.

In this study, it has purpose to develop an automatic grid regeneration program that automatically generates suitable grid for two-dimensional and three-dimensional solid-propellant rocket motors. To generate grids automatically, methods for automatically detecting poor grids and solving these problems without user intervention are needed. These methods are applied to the grid regeneration program. The several methods for improving the quality of the grid are introduced in this paper. In addition, the application of the developed grid regeneration program is conducted for several complex configurations and solid-propellant rocket motors. When the quality of the grid is checked in terms of skewness, better result can be obtained compared to the conventional methods. Since poor meshes are unexpectedly generated at the complex region, it can be applied to generate the grid of complex configurations.

Keywords : Solid-propellant Rocket Motor, Fluid-Structure Interaction, Viscous Grid, Boundary Layer, Automatic Grid Regeneration, Advancing-Layers Method

Student Number : 2016-20732

Table of Contents

Abstract i

Table of Contents iii

List of Figures v

List of Tables viii

Chapter 1 Introduction 1

1-1 The phenomenon of Solid-propellant Rocket Motor (SRM) 1

1.2. Simulation on Solid-propellant Rocket Motors 3

Chapter 2 Numerical methods for grid generation 9

2.1. Delaunay triangulation [10,12] 9

2.2. Bowyer/Watson Algorithm 10

2.3. Quad-Tree data structure and Oc-tree data structure 12

2.4. Grid untangling method 14

2.5. Advancing-Layers Method (ALM) 15

2.5.1 Advancing-Layers Method for two-dimension 16

2.5.2. Advancing-Layers Method for three-dimension 20

Chapter 3 Grid generation methods for internal flows 26

3.1 Grid generation method for internal flow for two-dimension 26

3.2 Three dimensional grid generation methods for internal flows 34

Chapter 4 Grid generation program 41

4.1. Linking process with FSI solver 41

4.2. Overall procedure of grid regeneration module 42

Chapter 5 Aplications 47

5.1. Applications on complex geometries 47

5.2. Applications on solid-propellant rocket motors. 49

5.2.1 Two-dimensional Solid-propellant rocket motor 49

5.2.2 Three-dimensional Solid-propellant rocket motor 56

Chapter 6 Conclusion 59

Appendix A. Advancing-Layers Method by Pirzadeh [19,21] 61

Appendix B. Skewness and Area/Volume ratio [24] 63
References 63
국 문 초 록 63

List of Figures

Fig. 1 Schematic diagram of burning process in the combustion chamber of SRM[5]……2

Fig. 2 Schematic diagrams of fluid-Structure Interaction and information exchange between fluid and solid modules [7,9]……4

Fig. 3 Example of prismatic meshes[12]……6

Fig. 4 Illustration of the Bowyer/Watson algorithm for Delaunay triangulations [10]……12

Fig. 5 Quad-tree data structure and its corresponding domain decomposition [14]……13

Fig. 6 Simple Oc- tree image(left) and its data structure(right)……14

Fig. 7 Schematic diagram of the grid untangling method[16]……15

Fig. 8 Setting the surface and point vectors……16

Fig. 9 Laplacian smoothing of surface vectors[19]……..17

Fig. 10 Example of grid generation in 3-D (sphere)……23

Fig. 11 Grid points connected to faces on the front by tension springs[17]……..24

Fig. 12 Example on loss of surface vector directionality in 2-D……28

Fig. 13 Stepwise smoothing method applied at above example……..28

Fig. 14 Grid generated in Pointwise T-Rex……..28

Fig. 15 Comparison of proposed grid generation tools for the 2-D test configuration……31

Fig. 16 Skewness histogram, (blue) Conventional Advancing-Layers Method, (red) Advanc ing-Layers Method for internal flow, (grey) Pointwise T-Rex……...…….……...31

Fig. 17 Poor meshes generated at the narrow region between generated meshes……32

Fig. 18 Grid generated by (a) in-code, (b) Pointwise T-Rex……...……33

Fig. 19 Poor grid at sharp region and skewness check……33

Fig. 20 Quality improvement after applying the skewness restriction……..……34

Fig. 21 Example of application of collision detection technique: 3D solid propellant shape (EBM) (top) Front cross-section (bottom) Side cross-section……34

Fig. 22 Examples of the blending mesh[23]……..……...35

Fig. 23 Conflict test at the corner (a) Conflict check only, (b) Shrinking method and (c) Skewness restriction……...36

Fig. 24 Spring analogy application example 1: (L) Before application, (R) After application

……..……36

Fig. 25 Spring analogy application example 2: (L) Before application, (R) After application ……..……37

Fig. 26 Application example: 3D solid propellant rocket motor configuration (EBM) (top) front-cross section (bottom) side-cross section……38

Fig. 27 Application example: 3D solid propellant rocket motor configuration (EBM) (top) front-cross section (bottom) side-cross section……39

Fig. 28 Skewness histogram (blue) in code, (red) T-Rex……..……..40

Fig. 29 process interacting information between the FSI solver and the grid regeneration module……41

Fig. 30 The overall flow chart of the grid regeneration……..42

Fig. 31 The flow chart of viscous grid generation……44

Fig. 32 Grid shrinking method……..44

Fig. 33 Three point sets (scanned data sets from surfaces) used for experiments……48

Fig. 34 Skewness distribution of AAM second stage……...49

Fig. 35 Histogram of the generated grid (a) skewness, (b) Area ratio……...50

Fig. 36 Pressure profile at the AAM outlet……...51

Fig. 37 Simulation results with time change (t=0.00s, 0.02s, 0.03s, 1.00s respectively)……52

Fig. 38 Temperature/stress contour before/after deformation……...……53

Fig. 39 Comparison with before/after conbustion of BCM at initial ignition and 0.824s after ignition……53

Fig. 40 Generated grid of BCM, (top) Initial ignition, (bottom) 0.824s after ignition…….54

Fig. 41 Histogram of skewness and area ratio of BCM……..55

Fig. 42 Mach contour configuration and detection of boundary layer at t=0s and t= 0.824s ……..55

Fig. 43 3-D configuration of Erosive Burning Motor……...……...56

Fig. 44 Temperature contour of numerical simulation result…...……57

Fig. 45 Change of fluid domain (L) at t =0s, (R) at t = 0.234s……...…….57

Fig. 46 Skewness histogram of EBM…….57

Fig. 47 Mach contour configuration and detection of boundary layer at (a) t=0s and (b) 0.234s ……58

Fig. 48 Steps of the advancing-layer method: (a) computation of boundary normals, (b) generation of a new layer and subdivision of the elements, (c) finished stretched grid, (d) generation of isotropic elements in the rest of the domain…….62

List of Tables

Table 1 Generalized staggered procedure……..4

Table 2 Main characteristics of grids for Solid propellant rocket motors……..5

Table 3 Characteristics of Delaunay triangulation……..10

Table 4 Procedure of Bowyer/Watson algorithm[13]……..11

Table 5 Input variables of grid generation for solid-propellant rocket model(ABM)……..29

Table 6 Comparison of three different mesh generation tools for the 2-D example configuration……...30

Table 7 Statistics of generated grids of in-code and T-Rex……40

Table 8 Surface grid information and user-defined information……43

Table 9 Information for post-process procedure……45

Table 10 Detailed techniques applied to the 2D and 3D grid generation modules……..46

Table 11 Statistics for generated grids of three test configurations……..48

Table 12 Statistics of generated Grid of AAM……50

Table 13 Algorithm settings for the FSI solver……51

Table 14 information of the generated grid before/after deformation……54

Table 15 Advancing-Layers Method by Pirzadeh……...61

Chapter 1

Introduction

In space launch vehicle and military weapon systems, propulsion systems are utilized in a variety of ways. Propulsion systems are mainly classified as the liquid-propellant rocket motor and the solid-propellant rocket motor. The liquid-propellant rocket motors contain complex structures and the liquid-propellant cannot be stored for a long period of time. However, it can be actively controlled in thrust and can generate relatively large thrust force. It is mainly used in main space launch rockets. On the other hand, the solid-propellant rocket motor is simple and has long-term storage. It is mainly used for auxiliary rockets and military weapons in space launch rockets[1]. However, it is very important to understand the combustion characteristics of the propellant and the physical phenomena inside the combustion chamber. In addition it is required to predict the performance of the system because the solid-propellant rocket motor cannot actively control the thrust force[2].

1.1 The phenomenon of Solid-propellant Rocket Motor (SRM)

The solid-propellant rocket motor burns the contained propellant grain in the combustion chamber and generates thrust by injecting high velocity gas through a supersonic nozzle. The internal combustion chamber of a solid propellant rocket motor is difficult to be predicted as a general method because of the complicated physical phenomenon from the behavior of the solid-propellant rocket motor having the unsteady flow at high temperature, high pressure and

the nonlinear viscoelastic characteristics[3]. Due to the nonlinearity and viscoelastic behavior of the propellant grain and hot exhaust gases formed during the burning process, complex multi-physical phenomenon occurs in the combustion chamber during the transient combustion process[4]. Research on solid-propellant rocket motor is mainly conducted through experiments. However, the research through experiments has many problems such as cost and stability. Because of the high temperature and high pressure combustion gas generated in the combustion chamber, research on solid-propellant rocket motor has limitation in the use of precise experimental equipment[4]. It is impossible to directly observe the internal physical phenomenon, mainly to obtain quantitative values such as internal pressure measurement and temperature measurement of the propellant.

As the military weapon systems and rocket propulsion industry steadily develop, more complex types of propulsion system are required. In order to develop propulsion systems, it is necessary to accurately predict the physical phenomena occurring in the combustion chamber. Therefore, various attempts have been made to analyze the physical phenomena inside the combustion chamber by using numerical analysis. A schematic diagram of a combustion chamber is shown in **Fig. 1.**

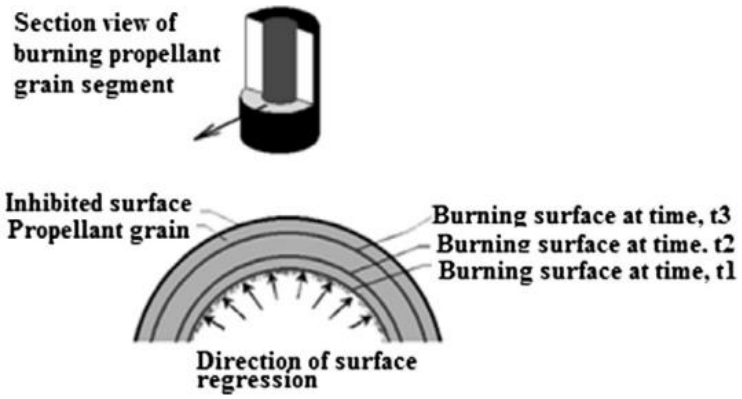

Fig. 1 Schematic diagram of burning process in the combustion chamber of SRM[5]

1.2. Simulation on Solid-propellant Rocket Motors

1.2.1. Fluid-Structure Interaction(FSI) analysis for Solid-propellant Rocket Motors

The solid-propellant is deformed over time from its initial configuration because the propellant is consumed during the combustion that is necessary to obtain thrust (propulsive) force. The combustion and the structural reaction of the propellant are fully combined in the solid-propellant rocket motor[6]. The burning rate in rocket motors running with solid-propellant is expressed as a regression from the combustion surface in terms of time [5].

It is difficult to predict the phenomenon of the inside (combustion chamber) of the solid-propellant rocket because of the force generated by the high pressure flow. The shape of the propellant is deformed by the load and the combustion that deforms the region of the internal flow in the combustion chamber.

The research on phenomenon of the combustion chambers of solid-propellant rocket motors has been focused on the field study in the individual interdisciplinary study rather than the multi-disciplinary study. Therefore, the necessary information in the field of relative inter-disciplinary was processed only by relatively simple input-output models, and thus there was a limit to simulate the multi-combined interference-effect of the actual phenomenon[7].

To understand the phenomenon accurately, fluid–structure interaction(FSI) analysis has been developed. FSI solves fluid formulas and structural formulas simultaneously where specific fluid variables serve as boundary conditions[8]. The FSI analysis is utilized in multi-disciplinary phenomena inside solid-propellant rocket motors. Simulation applying FSI analysis exchanges necessary information between fluid and structure interface. The process is shown in **Fig. 2**. In fluid and structural domains, the results interpreted by each analytical module affect each other through the information transferred at the fluid-structure interface. The process of exchanging

the information of fluid and structure region is called 'Generalized staggered procedure[9]' and the time-steps are accumulated through information exchange at the interface. The process at unit time-step is divided into 4 steps as shown in **Table 1** below.

Table 1 Generalized staggered procedure

Generalized staggered procedure
1. The position and velocity information of the interface calculated in the structure domain is transferred to the fluid analysis module.
2. Using the position and velocity information from the structure interface, the fluid analysis module performs a one-step time advance analysis in the fluid domain.
3. The pressure information of the calculated fluid-structure interface in the fluid domain serves as the traction information in the solid analysis module.
4. Using the information transferred from the fluid domain, the solid analysis module performs a one-step time advance analysis. This allows the entire analysis program to complete a one-time step advance analysis.

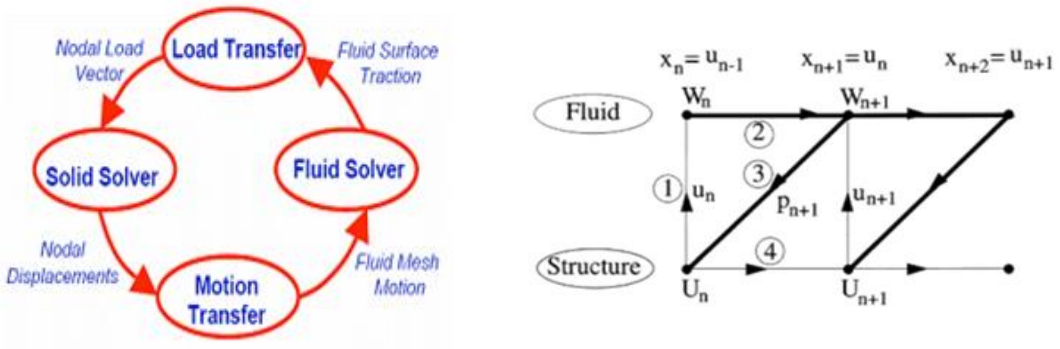

Fig. 2 Schematic diagrams of fluid-Structure interaction and information exchange between fluid and solid modules[7,9]

1.2.2. Grid Generation of Solid-propellant Rocket Motors

In the case of the solid propellant motor, the internal region of the motor continuously changes with the combustion of the propellant. Hence, grid generation techniques for the deforming region in the motor are needed. Because the internal flow of the solid-propellant rocket has high temperature and viscous flow, it is necessary to generate the viscous grid. In order to improve the accuracy of the analytical results, the grid quality should be kept high. In continuously changing analytical regions, grid regeneration techniques should be used to maintain the quality of the grid for improving the accuracy of the analysis result. For this reason, methods to automatically detect poor meshes and improve their quality are needed. Automatic-improvement methods of the grid quality are applied to the grid regeneration technique.

In the solid-propellant rocket motor, it is necessary to create grids suitable for the configuration in which the analysis region is deformable. In addition, it is necessary to generate grids suitable for the boundary layer for the efficient and accurate viscous flow analysis. Because the solid-propellant rocket motors have complicated configurations, they require unstructured grid generation methods that are easy to generate grids in complicated configurations[10] and require anisotropic grid generation to analyze viscous flows at high temperature and high pressure[4,12].

Table 2 Main characteristics of grids for the solid propellant rocket motors

Grid type required in solid propulsion analysis
Feature 1: complex and changing geometry → unstructured grid **Feature 2**: high temperature / high pressure of viscous flow → anisotropic grid (the grid that has high aspect ratio)

Various methods have been developed for the grid regeneration method. The most basic and stable method is triangle/tetrahedral grid. Triangle/tetrahedral grid provides flexibility in two- and three-dimensional grid generation because they can cover complicated topologies more easily compared to the quadrilateral / hexahedra meshes. In addition to greater flexibility in discretizing complex areas, triangle/tetrahedral grid can also directly implement adaptive mesh technology to add, remove, or move mesh points while the mesh connection is being updated locally to increase the quality of the grid[10].

However, the generation of triangle/tetrahedral grid for boundary layers is quite difficult. In the region of boundary layer, the main solution gradients occur in the direction normal to the surface, which requires meshes of very large aspect ratio. It appears that grids that have high aspect ratio are superior in capturing the directionality of the flow-field over viscous regions. A compromise between the two different types of grids is the mixed grid. The mixed grid consists of triangular faces that cover the body surfaces, while quadrilateral faces extend in the direction normal to the surface. The meshes can have very high aspect ratio, while providing geometric flexibility in the lateral directions. The shape of that mesh is like a 'prism'. An example of a prismatic grid is shown in **Fig. 3**[12].

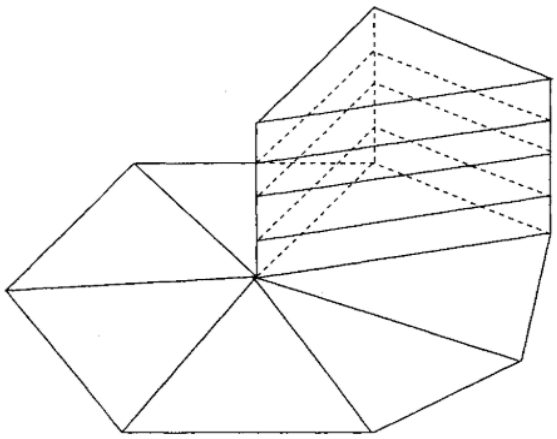

Fig. 3 Example of prismatic meshes[12]

The inside of the combustion chamber is divided into the propellant region and the fluid region.

Each region changes over time by the combustion of the propellant. The thrust force of the rocket outlet is dependent to the area of the interface where the flow region and propellant region contacts. Various types of propellant distributions have been developed to control the thrust force.

To increase the thrust force of the rocket outlet, complex propellant distributions are designed to widen interface area. As propellant distribute is more complicated, the internal flow regions also become complex. Therefore, for the analysis of this phenomenon, it is necessary to consider the continuous change of the flow-structure interface because of the combustion process and the complex internal structure. In addition, the flow geometry changes over time and requires the suitable grid for every feature. To do this, grid regeneration is required to generate suitable grids for deformable geometry.

Prior to the analysis of a solid-propellant rocket motor, it requires techniques of generating grid suitable for changing shapes. Since the solid-propellant rocket motor has complicated configurations, it requires unstructured grids that are easy to generate grid in complicated configurations and requires viscous grid generation to easily analyze viscous flows at high temperature and high pressure.

In the case of grid generation on complex internal flows such as solid-propellant rocket motors, overlap between inner grids occurs in the process of automatic generation of the grid, or inevitably poor meshes can be generated. A method to automatically detect and solve these problems is needed, and automatic grid improvement method is applied to the grid regeneration technique.

This paper presents approaches to the problems about grid generation that is suitable for a solid-propellant rocket motor. In Chapter 2, conventional grid generation techniques are introduced. Chapter 3 describes methods for grid generation for internal flow. Some problems of the grid generation of solid-propellant rocket motors are introduced and several methods to

solve the problems are described. The whole program including conventional grid generation methods and modified methods for internal flow is introduce in Chapter 4. Chapter 5 presents the examples applied to the numerical analysis of the solid-propellant rocket motors. The grids generated by the program for the configuration of solid-propellant rocket motors are analyzed using the integrated FSI solver.

Chapter 2

Numerical methods for Grid regeneration

Among the conventional grid generation methods, the techniques for the grid regeneration are introduced in Chapter 2. Conventional grid generation methods have been developed primarily for external flows such as airfoils.

The Advancing-Layers Method[17, 19, 21] and the Delaunay-triangulation using the Bowyer-Watson algorithm[10-12] are used to generate unstructured grid that contains the anisotropic grid and the triangular(2-D) / tetrahedral(3-D) grid. It applies the Advancing-Layers method for viscous grid generation for boundary layer and Delaunay triangulation for triangular/tetrahedral grid at the remaining region. The unstructured grid information is stored in quad-tree or Oc-tree data structures to efficiently find data.

2.1. Delaunay triangulation [10,12]

Delaunay triangulation is utilized to the points given in the space to describe the fact that it does not include any other points in the circumscribed circle for each triangle or tetrahedron constructed by uniquely configuring triangles in two dimensions and tetrahedral in three dimensions respectively. In the Delaunay triangulation, point distribution is given to the Voronoi diagram which is geometrical dual relation to Dirichlet tesselation. The Voronoi diagram is the optimized distribution in a given configuration. Mathematically, Delaunay triangulation can be expressed as

$$H_{ij} = \{x \in R^3 \mid d(x, P_i) \leq d(x, P_j)\} \quad (1)$$

The distance between a point in space and nearby point is denoted by $\boldsymbol{d(x, P_i)}$. The partitioned Voronoi diagram is a geometric dual with the Delaunay triangulation. In the Voronoi diagram, the Delaunay triangulation is formed when the points having tangent faces are connected. Delaunay triangulation in two- and three-dimensional configurations has the following properties.

Table 3 Characteristics of Delaunay triangulation

Delaunay triangulation
1. Delaunay triangulation maximizes the minimum angle of the triangle
2. Delaunay triangulation does not include any other points in the circumscribed circle. This is called 'empty circumcircle characteristic' and the process of confirming it is called 'Delaunay test'.
3. When a new point is added to a space other than a given point, the initially constructed Delaunay triangle violates the empty circumcircle characteristic condition. At this time, if a triangle having a circumscribed circle including a new point is deleted, a cavity is created, and each point located on the cavity space and the newly added point can be connected by straight lines.
4. The newly added points and the points forming the common space constitute a new triangle, and the newly constructed triangles satisfy the conditions of the Delaunay triangulation.

2.2. Bowyer/Watson Algorithm

One of the simple and effective methods for Delaunay triangulation is the Bowyer / Watson algorithm. If a new point is added or a point in the circumscribed circle is found, search for surrounding triangles is performed to find and delete triangles that do not satisfy the circumscribed characteristic. Then the new points and the cavity points are connected and become triangles[19].

The techniques are utilized to guarantee the circumcircle characteristic of the triangles that make up the Delaunay triangulation and satisfy requirement of B/W algorithm when additional points are no longer needed[13].

Table 4 Procedure of Bowyer/Watson algorithm[13]

Basic steps of Bowyer/Watson Algorithm
1. The points that make up the interface are specified.
2. The initial triangulation process is performed using the boundary points.
3. Search for the area of the constructed triangle where additional points are needed is performed.
4. After adding new points, the triangulation process using Bowyer / Watson algorithm is performed and information about new points in data tree data is stored.
5. Steps 3-4 are repeated until no further points are needed.

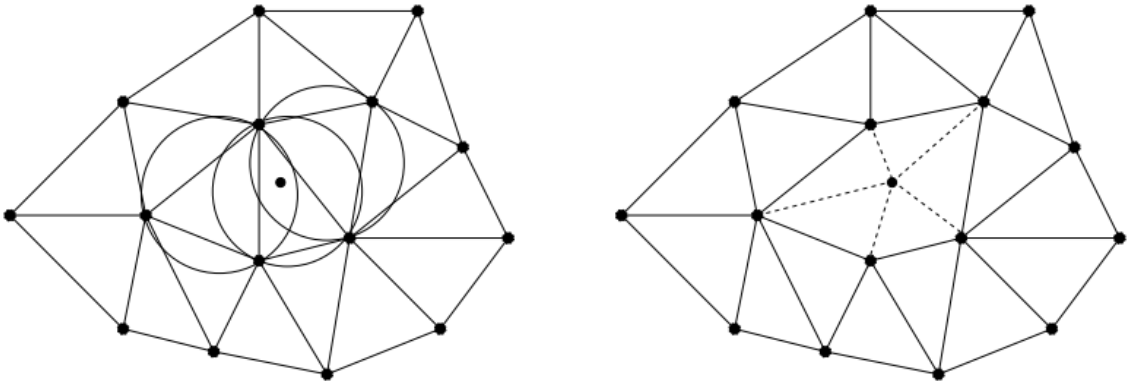

Fig. 4 Illustration of the Bowyer/Watson algorithm for Delaunay triangulations [10]

2.3. Quad-Tree data structure and Oc-tree data structure

Compared to the structured grid, which can easily find the positional relationship between the points through the indexes of the grid points, the unstructured grid requires additional information to store the positional relationship between neighborhood cells. The grid generation technique used in this study has a great effect on the efficiency of calculation when the new circumference includes adjacent points. If a search is performed without a special information structure, all triangles must be examined, and the number of execution tasks is $\mathbf{O}(\boldsymbol{N^2})$**,** where N is the number of points in the unstructured grid. When using quad-tree data structure, this operation is reduced to $\mathbf{O}(\mathbf{NlogN})$**[14]**. The data structure has the advantage that quickly find the closest point to a point.

In one area, more than four points cannot be stored, and when more points are stored, they are divided into four sub-areas. As a result, one point stores the unique information of the point and the information of the region to which the point belongs (top-to-bottom relationship between regions, the number of points contained in the region, etc.). This makes it possible to efficiently find the position information necessary for the calculation of the unstructured grid.

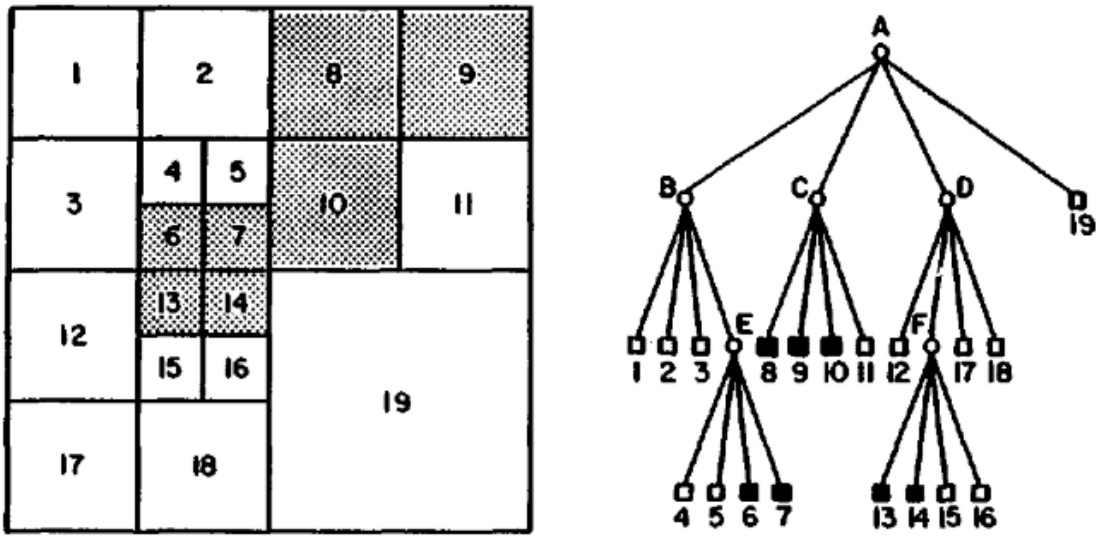

Fig. 5 Quad-tree data structure and its corresponding domain decomposition [14]

In three-dimension, the Oc-tree data structure can be used instead of the Quad-tree data structure. It is one of tree data structures in which each internal node has exactly eight sub-areas. The Oc-tree data structure is most often used to partition by recursively subdividing it into eight octants. When using the Oc-tree data structure, search for neighbor points and neighbor volume meshes in the unstructured grid has the advantage that quickly finds the closest point to a point. This makes it possible to efficiently find the position information necessary for the calculation of the unstructured grid for three-dimension[15].

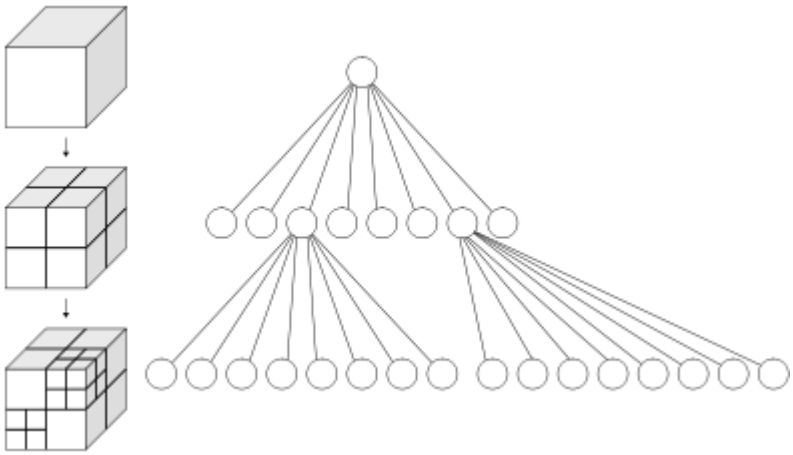

Fig. 6 Simple Oc- tree image(left) and its data structure(right)

2.4. Grid untangling method

When the viscous grid is created, the grid generated at the sharp region often incurs grid-overlap or the poor quality of the grid at that region is generated. To remove such overlap, an edge-based limiter for the prismatic layer height is applied.

For each edge **e** of the wall mesh, $\boldsymbol{\beta 1}$ and $\boldsymbol{\beta 2}$ are the angles between the edge direction and the vertex normal vectors in the end of the edge. Using $\boldsymbol{\gamma = \pi - \beta 1 - \beta 2}$, the maximum allowable height at the edge end-point j is then obtained[16] from

$$\boldsymbol{h_j < |e| \text{ where } 0 < \gamma < \pi} \qquad (2)$$

In this way, the grid untangling method can prevent the grid from overlap at sharp regions. The schematic diagram of the grid untangling method is shown in **Fig 6**.

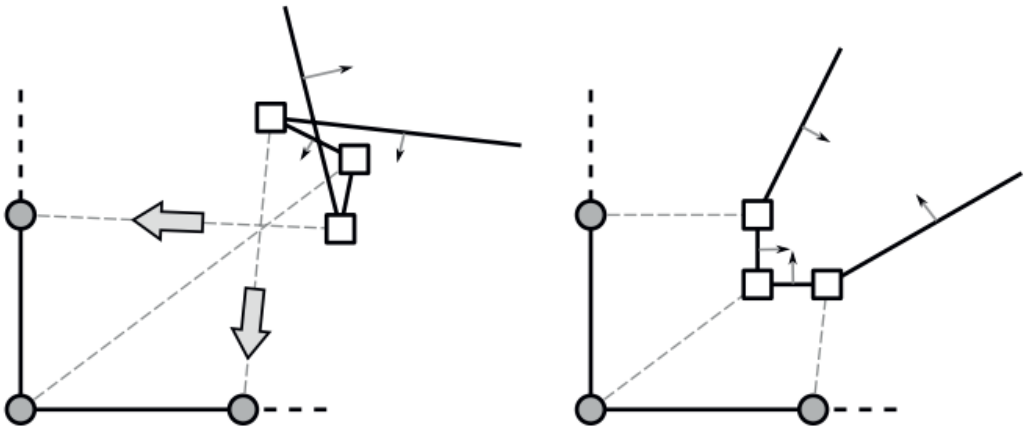

Fig. 7 Schematic diagram of the grid untangling method[16]

2.5. Advancing-Layers Method (ALM)

The lack of the triangle/tetrahedral grid generation for highly stretched cells has been a major obstacle to apply grid generation methods to complex viscous-flow problems[17]. An alternate approach to the problem of viscous unstructured grid generation is the Advancing-Layers Method. Advancing-Layers Method is a technique for producing thin-layered prism grids suitable for computation of viscous fluid flows[17,18].

The Advancing-Layers Method(ALM) is similar to the hyperbolic structured grid generation technique[18]. ALM has marching grid generation techniques by layering on the surface of the boundary. This grid generation method can overcome the complexity of the grid boundary. The process of viscous grid generation through the ALM is briefly shown in **Appendix. A[19].**

2.5.1 Advancing-Layers Method for two-dimension

The two-dimensional Advancing layer method is a method of generating a grid by matching the triangular unstructured grid with the quadrilateral grid of the viscous grid region. The basic process of generating viscous grid is introduced below.

(1) Basic steps of Advancing-Layers Method [21]

1) Determination of initial boundary face

The distribution of the initial boundary face is determined by the importance on the accuracy of computation. To determine the appropriate number of boundary points is important for the efficient computation.

2) Setting the surface vector

ALM creates a new grid point according to the direction of the surface vector and efficiently obtains a suitable grid without complicated process. The surface vectors are determined from vertical vectors of the edge on the surface of the configuration to the computation domain. Point vectors are determined to the average value of the two surface vectors that are tangential to faces of the intermediate points.

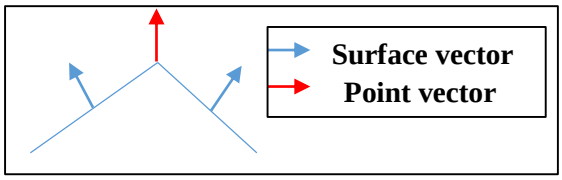

Fig. 8 Setting the surface and point vectors

3) Laplacian Smoothing process of surface vector

The initially determined point vector is distributed only in the vertical direction of surface edge. However, in several cases, it intersects with the adjacent surface vectors. Therefore, smoothing process is needed to obtain uniform grid distribution for the advancing-layers method. The smoothing process utilizes the Laplacian smoothing method through iterative calculation.

$$\boldsymbol{v_p^{t+1} = (1 - w)v_p^t + \frac{w}{N_p}\sum_{n=1}^{N_p} v_n^{t-1}} \quad (3)$$

where $\boldsymbol{v_p}$ is a surface vector at grid point $\mathbf{p}$, $\boldsymbol{v_n}$ is a vector at the $\boldsymbol{n_{th}}$ neighboring point at point $\mathbf{p}$, $\mathbf{w}$ is a relaxation parameter($\mathbf{0 < w < 2}$), $\mathbf{t}$ is an iteration level and $\boldsymbol{N_p}$ is the number of points connected to point $\mathbf{p}$.

(a) face normal vectors

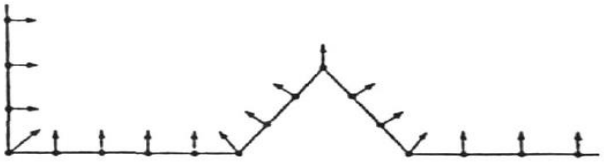

(b) vectors at surface grid points before smoothing

(c) vectors at surface grid points after smoothing

Fig. 9 Laplacian smoothing of surface vectors[19]

4) Determining the spacing of the advancing layer

As the new grid points are generated along the surface, the interval spacing of advancing layer is determined by the value from a specific function. The position of newly generated points is determined by the specific stretching function. The shape of the viscous grid can be adjusted through the initial advancing spacing and growth rate. The grid spacing for advancing layer increases exponentially as the advancing process goes over. The stretching function is used as

$$\boldsymbol{\delta_l = \delta_1(1+r)^{l-1}} \quad (4)$$

where δ_l is the spacing for the l_{th} layer, and r is a prescribed rate of stretching across the boundary layer. The spacing for the first layer of cells, δ_1, is also prescribed by the user.

(2) Spring analogy

Maintaining the isotropic of the unstructured grid is important to improve the quality of the grid. In order to obtain the optimum point at the grid generation, spring analogy is used. The candidate points are assumed to be connected to the neighboring points by tension springs[17]. The spring analogy optimally determines the point at which the elastic force is the smallest among the points on the surface of the object. For the system to be in equilibrium, the force at every point **p** has to be zero[20]. Standard proportional expression of the spring analogy is shown as

$$\boldsymbol{F_p \propto \sum_{n=1}^{N} s_n} \quad (5)$$

where $\boldsymbol{F_p}$ is the total force exerted on point **p**, $\boldsymbol{s_n}$ is the distance by which the $\boldsymbol{n_{th}}$ spring connected to point **p** is stretched from its neutral length, and **N** is the number of spring

connected to point **p**. Among the candidate points, the one with smallest $\boldsymbol{F_p}$ is selected to form the next cell[19, 22].

It is possible to eliminate cross(conflict) check procedure between the near meshes, which has a long time consuming process. In two-dimension, the above proportional expression can be transformed as

$$\mathbf{max}\left(\boldsymbol{F_{AB}^{A'}}, \boldsymbol{F_{AB}^{B'}}\right) > \ \mathbf{min}\left(\boldsymbol{F_{CD}^{A'}}, \boldsymbol{F_{CD}^{B'}}\right) \qquad (\mathbf{6})$$

where $F_{AB}^{A'}$ represents the elastic force between a point A' and a front edge AB**.**

(3) Advancing stop condition

As the viscous layer accumulates, the grid generation stops in certain condition. First, when spring analogy condition is not satisfied, advancing procedure at the edge is stopped. The spacing between adjacent meshes from the front edge is determined by using spring analogy. Because the spacing of the first boundary layer is user-defined, the grid can be smoothly generated. Secondly, when the number of advancing steps exceeds the user-defined maximum advancing step, the generation of the viscous grid stops.

2.5.2. Advancing-Layers Method for three-dimension

In the three-dimension, a grid is created by the ALM method mainly similar to the two-dimensional process. However, due to problems in three-dimensional configurations, it must go through several different processes. First, in the case of a surface vector in a sharp part or an edge part, in the method used in the two dimensional ALM, the shape of the mesh is destroyed and the negative volume of meshes can be obtained. However, in the case of three-dimension, the grid should be arranged in order to match connection state. Unlike the two-dimensional case, the unstructured grid generation for three dimension requires the renumbering process for the grid points and the connection state.

(1) Basic steps of Advancing-Layers Method [17]

1) Determination of surface vector

In the two dimensional surface vector determination process, the value obtained by taking the average of the surface normal vector is determined as the surface vector, in the case of three dimension, however, volume grids are generated through complicated processes. Because of the surface of the object is a simple line in the two-dimensional case, the connected point at a point is always two. Therefore, the surface vector for each grid point can be simply obtained by calculate the simple average of the surface vector.

On the other hand, in the case of 3D, the surface corresponds to the plane and is surrounded by a different number of the grid points because of the unstructured grid. the surface vector is determined depending on the number of grid points connected regardless of the surface.

In the unstructured method for three-dimension, the point distribution is unaligned. If

distribution is unaligned, surface vectors may point wrong direction. To solve this problem, the following method is used. The most important factor in three-dimensional surface vectors is the visibility condition of the surface vector. Visible conditions prevent the creation of the grid of negative volume which can be caused by the surface vector, provided that the surface vector of the point must be visible on the grid face surrounding a certain point. When expressed as a vector expression

$$\boldsymbol{v_p \circ n_f = c; f = 1, 2, \dots, F_t} \quad (7)$$

where c is the visibility constant and must always be greater than zero. The above conditions can be obtained through the following iterative process.

① v_p is obtained by the weighted average.

$$\boldsymbol{v_p^t = \mathrm{w} \sum_{f=1}^{F_t} w_f^t n_f + (1 - w) v_p^{t-1}} \quad (8)$$

② The deviation between the angle formed by the surface vertical vectors v_p and n_f and the average angle is obtained.

③ The new weight function to use in the next step is shown as

$$\boldsymbol{\bar{w}_f^{t+1} = w_f^t (1 - \frac{\delta_f}{\bar{a}})} \quad (9)$$

④ The weight function is modified with the new weight function:

$$\boldsymbol{w_f^{t+1} = \bar{w}_f^{t+1} (1 - \sum_{f=1}^{F_t} \bar{w}_f^{t+1})} \quad (10)$$

⑤ The above procedure is repeated until the variation of v_p becomes small.

The surface vectors obtained by the above method generate the grid by utilizing the Laplacian smoothing. Then all surface vectors are defined for each grid point on the surface. The calculated surface vectors are used to generate a grid by using the advancing procedure.

2) Determining the spacing of the advancing layer [17,22]

The process of generating a three-dimensional grid proceeds in the same manner as a two-dimensional grid generation method. However, the spacing of the advancing layer does not increase at a constant growth rate unlike the case of the two-dimensional structure. Because the two-dimensional viscous grid does not have a large number of grid points, a sufficient number of layers are possible in the boundary layer region, however, an excessive number of the grid can be generated. The size of the advancing step is calculated based on a user-defined spacing of the first layer and on growth rate in the normal direction. The spacing can be defined as

$$\Delta \boldsymbol{n_k} = \Delta \boldsymbol{n_0}\left[\mathbf{1} + \boldsymbol{a}(\mathbf{1} + \boldsymbol{b})^{\boldsymbol{k-1}}\right]^{\boldsymbol{k-1}} \quad (\mathbf{11})$$

where Δn_0 is the given first layer thickness, Δn_k represents the spacing of the k_{th} layer and $0.04 \leq a \leq 0.2$ and $0 \leq b \leq 0.07$ stand for the stretching parameters. When the grid is formed by the above method, the advancing layer is increased at a low rate of increase around the surface and stacked up rapidly as the distance from the surface increases.

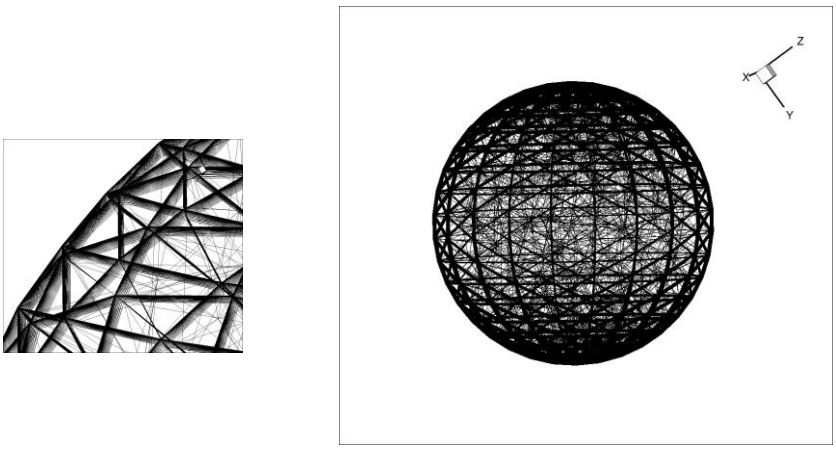

Fig. 10 Example of the viscous grid generation in 3-D (sphere)

3) Advancing-stop condition

The advancing stop condition of the three-dimensional grid generation is similar to that of the two-dimensional case. The closeness to the adjacent planes is based on the spring analogy.

In the figure, A-B-C represents the current grid front, and D-E-F represents the grid-front on the adjacent boundary. The spring analogy used as follows.

$$F_p \propto \frac{1}{r_f} \sum_{n=1}^{N} s_n \qquad (12)$$

In the case of **Fig. 11**, the generation of the grid is stopped when the following condition is satisfied[17].

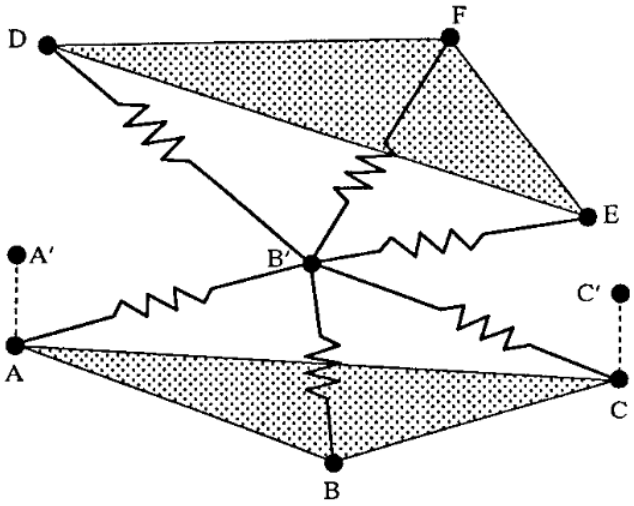

Fig. 11 Grid points connected to faces on the front by tension springs[17]

$$\max\left(F_{ABC}^{A'}, F_{ABC}^{B'}, F_{ABC}^{C'}\right) > \min\left(F_{DEF}^{A'}, F_{DEF}^{B'}, F_{DEF}^{C'}\right) \quad (13)$$

If all the grid on the front satisfy the stop condition, it is automatically switched to the unstructured grid generation as same in the two-dimension case. The meaning of is to stop the generation of grid when the grid surface repulsion is larger than the repulsion of the grid surface.

(2) Ancillary procedures for the ALM in three-dimension

1) Input process of surface information

In case of three-dimensional grid generation, it is important to efficiently store information of the grid and the point connectivity because the connection relation is more complicated than in two-dimensional case. The information about the surface grid is composed of the grid number, the coordinates of the points, the patch number, and the information of the viscous grid. The information about the viscous grid contains the information of viscous grid generation region, the spacing (thickness) of the first viscous mesh and the growth rate of the marching layer and the boundary patch number for marching process.

2) Organizing the information of grid connections

In the case of three-dimension, it is important to efficiently store the connection-relations between the meshes. First, it is efficient to accumulate the connection relation of the surface grid and proceed with the grid generation based on the relation.

The information generated in the grid generation process includes the relationship (cell to cell) between the surface grid and the grid which contact with surface grid, the relationship between the surface grid and the points constituting the grid, the relationship between the grid point and the adjacent node, and updates information on the front grid when advancing. updates information on the front grid is needed to check the collision while generating the grid.

In addition, the grid information is newly stored while generating the volume grid from the surface grid. A cell-cell relationship between a grid and an adjacent grid, and a relation (cell to node) between neighboring grid points including a grid. Especially, because the three dimensional grid has various types of shapes (tetrahedral, prism, pyramid, etc), data structure should consider these grid shapes.

3) Tetrahedral mesh generation tool

After viscous grid elements are generated in the region between wall and envelope layer, tetrahedral elements are created in the space between the viscous grid boundaries. The efficient tetrahedral mesh generation program, TETGEN developed by Han Si[22] is employed for tetrahedral mesh generation. TETGEN utilizes Delaunay tetrahedralization and adaptive quality tetrahedral mesh generation to generate tetrahedral grids.

Chapter 3

Grid generation methods for internal flow

In the case of external flow, Overlap between adjacent grids rarely happens. However, grid-overlap often occurs when the conventional grid generation is applied to the internal flow such as solid-propellant rocket motors.

This paper presents several problems when applying grid generation method to internal configurations. The modified methods are introduced to solve these problems.

3.1 Grid generation methods for internal flow for two-dimension

In two-dimension, problems are examined in generating a grid for the internal flow**.** One of the problems that occur at the internal flow is that the original direction of the surface vector has been lost during the smoothing process. If the ALM is applied to create the grid for the internal flow configurations, the surface vector eventually has wrong direction at the sharp point.

The reason is that conventional ALM continues the smoothing process until the surface vector converges. In the smoothing process, the original direction of the vector is lost, overlap between adjacent meshes can be generated and distorted meshes appear in that region in **Fig. 12.** In internal flow, because there are many sharp parts compared to external flow, additional treatments for keeping originality of vectors at the sharp region are needed.

In order to solve this problem in case of two dimensions, the stepwise smoothing process is applied without converging the direction of the vector at once. Initially, the direction of the

surface vector is maintained. However, the smoothing process gradually increases their iteration-times. In order to induce change in the vector direction, relationship between the number of advancing steps and the number of smoothing steps can be specified. If the following exponential relation can be adjusted, the directions of the vectors gradually become more smoothed directions. Compared to **Fig. 12**, the grid quality can be improved at that region.

To verify the above method, the grid in **Fig 12** is compared to the grid generated by other baseline program. Pointwise T-Rex is opted for the baseline program. Pointwise T-Rex ver. 18.0 R2 is used as automatic grid generator. Pointwise is a software system for the generation of two-dimensional and three-dimensional grids. Many grid generation methods used in Pointwise have been developed and fine-tuned. Pointwise's main viscous grid generator, *T-Rex*[24] generates anisotropic layers easily from the boundaries of unstructured domains. T-Rex program is commonly used as an automatic viscous grid regenerator. T-Rex has the advantage of generating a viscous grid. **Fig. 14** is a grid generated by T-Rex program under the same input conditions. It can be seen that the grid generation is similar when compared to **Fig 13**.

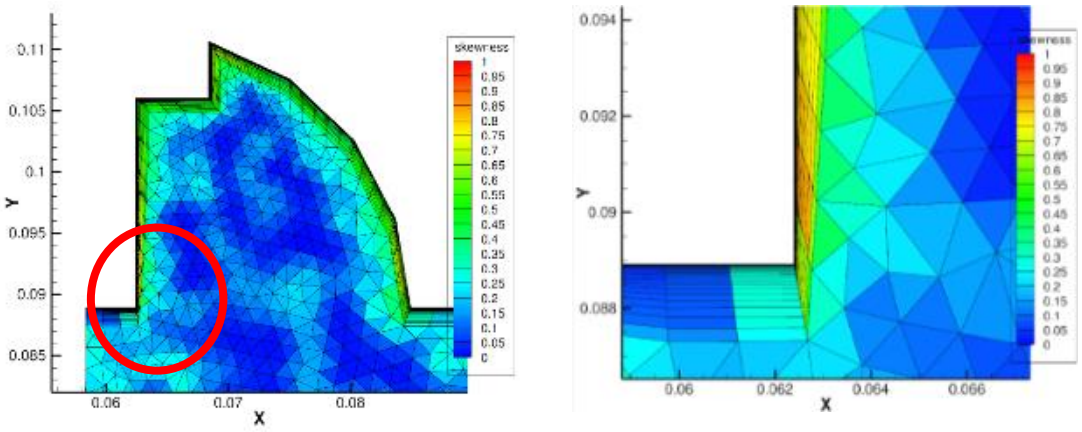

Fig. 12 Example on loss of surface vector directionality in 2-D

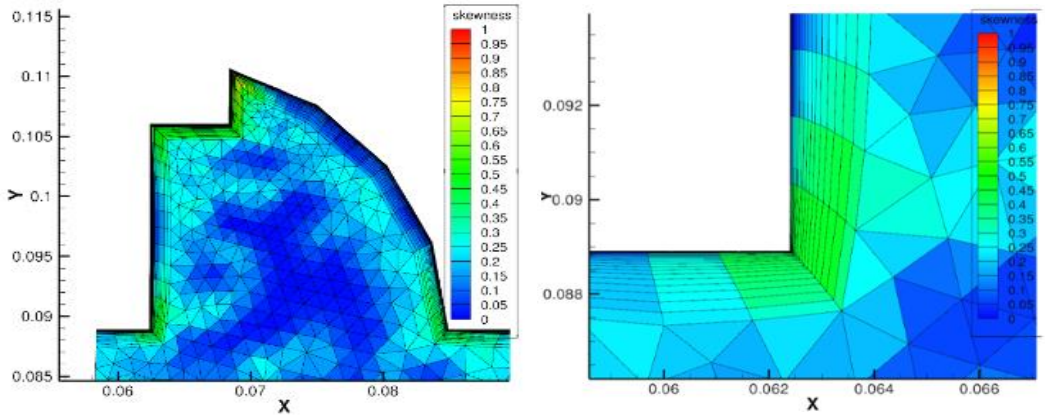

Fig. 13 Stepwise smoothing method applied at above example

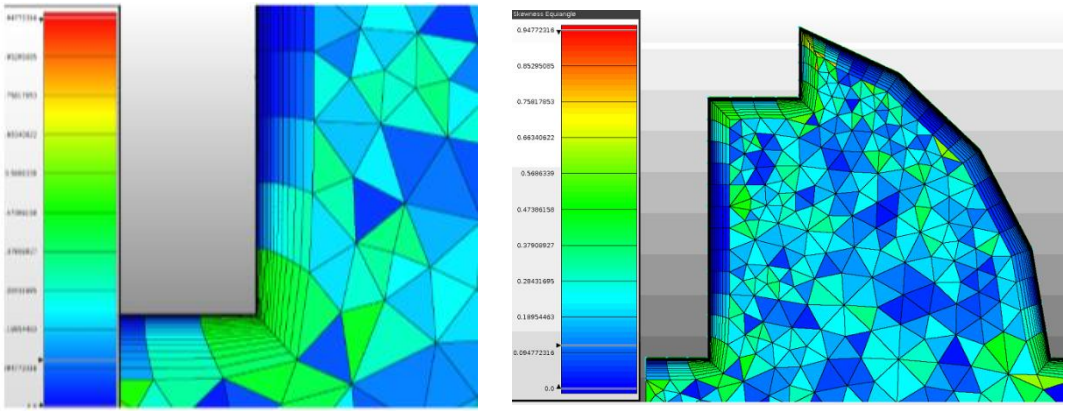

Fig. 14 Grid generated in Pointwise T-Rex

Using the proposed grid generation tools, the generated grids are compared and analyzed. The grids are generated by three methods: (a) conventional Advancing-Layers Method, (b) modified Advancing-Layers Method for internal flows and (c) Pointwise T-Rex. Comparison is made for the grids generated with the same configuration and input variables. The configuration is an example of the two-dimensional solid-propellant rocket motor, Anti-Ballistic Missile(ABM). The input variables of the point-distribution of the surface boundary, the number of the advancing-steps of the grid points and the spacing parameter of the first boundary layer mesh from the boundary wall are the same value in cases (a), (b), (c) as shown in **Table 5**. The quality of the generated grid is analyzed by the skewness factor. Skewness is a numerical factor that determines the quality of the grid and has value from 0 to 1[24]. The closer the skewness is to zero, the better the quality of grid is. Details on skewness are detailed in **Appendix B**.

Table 5 Input variables of grid generation for solid-propellant rocket model(ABM)

Model	ABM (Anti-Ballistic Missile)
The number of Input points	1353
Advancing step	20
Spacing of the first BL cell	$\mathbf{6.0 \times 10^{-6}}$

Fig. 16 is a skewness histogram comparing these methods: (a) Conventional Advancing-Layers Method, (b) Advancing-Layers Method for internal flow, (c) Pointwise T-Rex. In **Table 6**, the grids generated by three grid generation tools are compared. It can be confirmed that the quality of the grid is similar in (b), (c). The skewness average (b) shows that the average quality of the grid is better. It is confirmed that method (b) using the stepwise smoothing produces slightly suitable grid compared to other methods.

Table 6 Comparison of three different mesh generation tools for the two-dimensional example configuration

	(a)	(b)	(c)
The number of the grid	**41,302**	**42,139**	**40,174**
Skewness < 0.5 (%)	**98.71**	**99.91**	**99.86**
Skewness < 0.75 (%)	**99.82**	**99.99**	**99.98**
Average skewness of total grids	1.03×10^{-1}	8.51×10^{-2}	1.09×10^{-1}

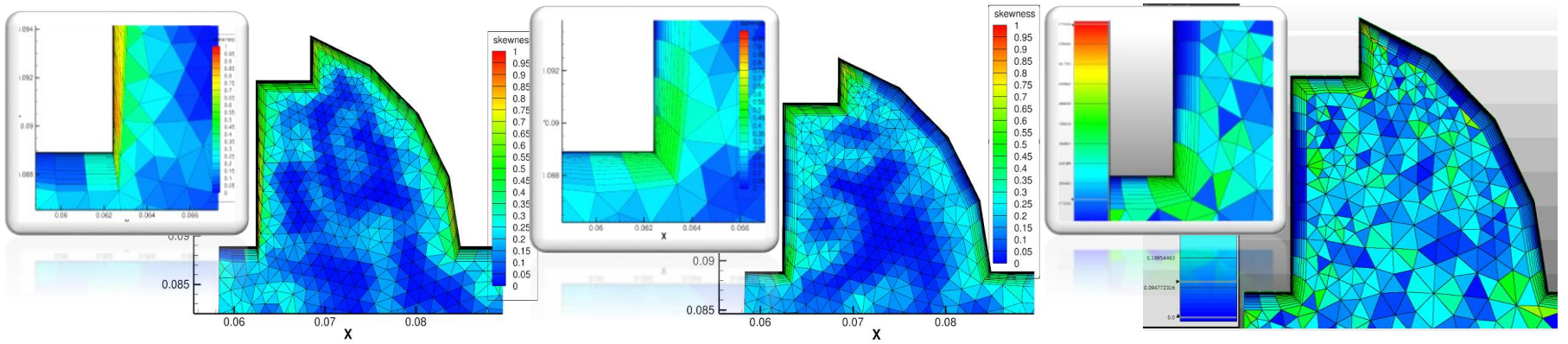

Fig. 15 Comparison of the proposed grid generation tools for the test configuration

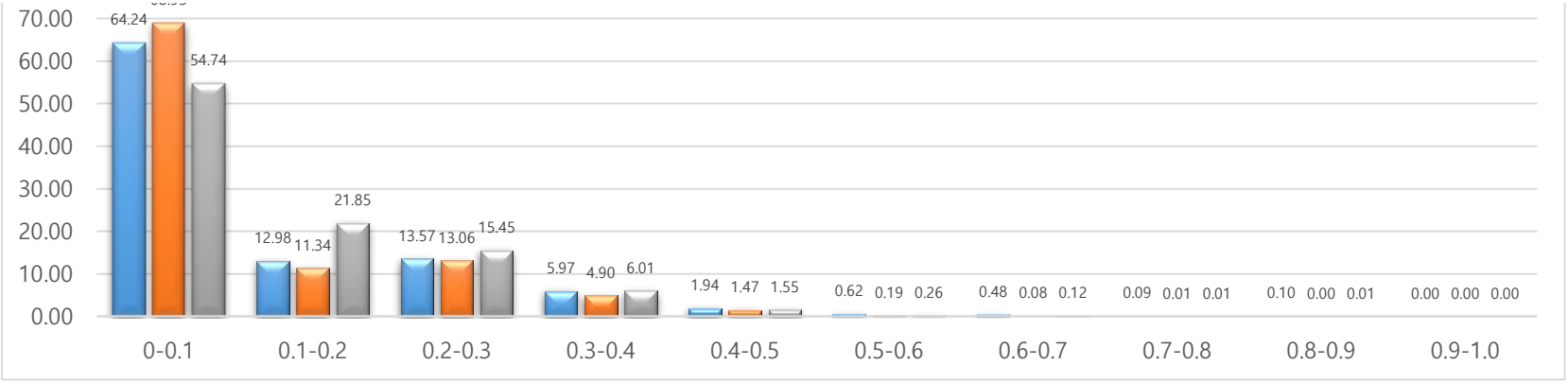

Fig. 16 Skewness histogram,

(blue) Conventional Advancing-Layers Method, (red) Advancing-Layers Method for internal flow, (grey) Pointwise T-Rex

When conventional viscous grid generation methods are applied to complex configurations, two main problems occur. First, it takes considerable computational time to check the collision on a one-to-one basis between collisions. In order to solve this problem, the quad-tree data structure is used. If the information of the grid is stored in the quad-tree data structure, the way to find adjacent grids becomes simpler and the computational time is shortened. Second, the generated grids by the collision detection are often produce too close to each grid. In **Fig. 17**, the quality of the grid becomes poor when the grid is generated in the narrow region. Therefore, it is necessary to secure space between the viscous meshes.

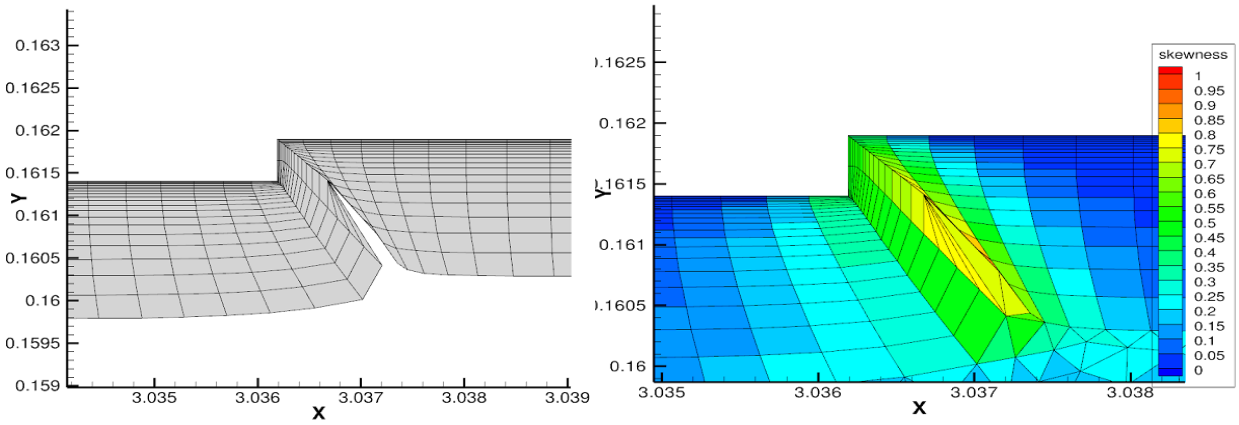

Fig. 17 Poor meshes generated at the narrow region between generated meshes

The grid shrinking method is a methodology to remove the grid by adjusting the grid advancing step smoothly to maintain the distance between adjacent grids. By applying this method, it is possible to secure space between the generated viscous meshes. The quality of the generated grid can be improved. **Fig. 18** compares the commercial program with the modified method. (a) is the generated grid in the modified method. (b) is the grid generated by Pointwise T-Rex. Appearance of the grids from different tools is similar each other.

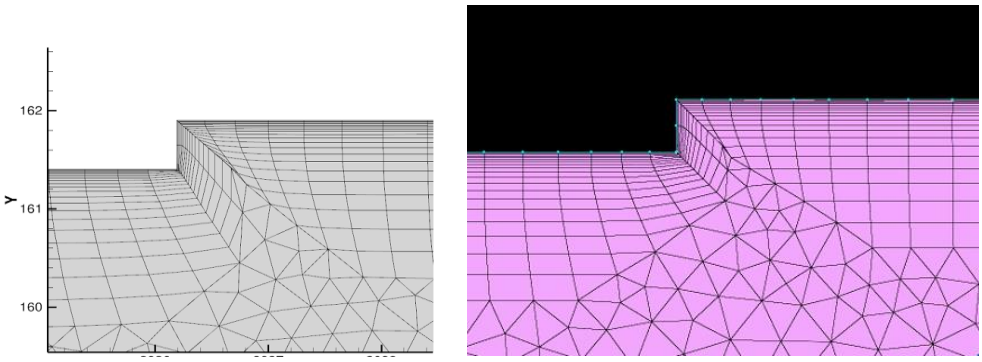

(a) (b)

Fig. 18 Grid generated by (a) the code using the modified method, (b) Pointwise T-Rex

In **Fig. 19**, it can be seen that the quality of the generated grid is poor at the region where meshes are approaching closer. The skewness of the region that checked in left side of **Fig 19.a.** The quality of the grid is poor in **Fig19.b**. To solve this problem, the skewness restriction is added.

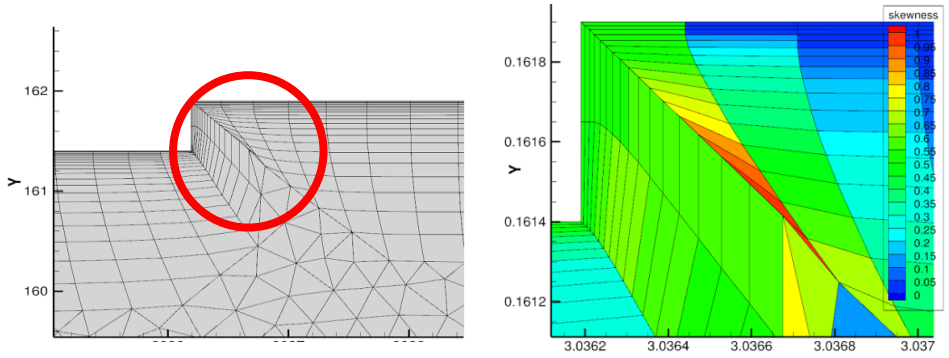

(a) (b)

Fig. 19 Poor grid at sharp region and skewness check

The skewness restriction is a method for the complex geometry. When the quality of meshes becomes worse than a certain level, the method prevents that the meshes are generated. The grid generated with the skewness restriction is shown in **Fig. 20.** The allowable skewness is limited by 0.5. The grid is prevented from overlap and secure the space of the triangular grid to improve the quality of the grid by using the skewness restriction. Compared to **Fig 19.b,** the meshes that have bad quality is generally removed.

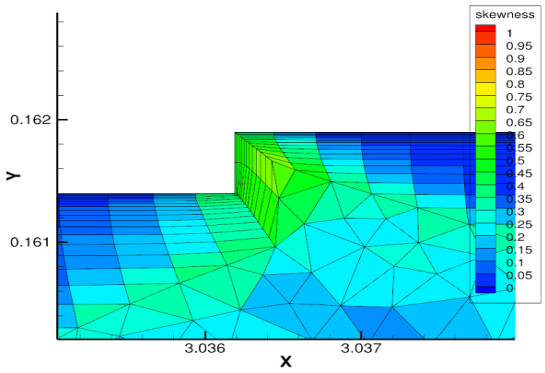

Fig. 20 Quality improvement after applying the skewness restriction

3.2 Three dimensional grid generation methods for internal flow

In three-dimension, there is a problem that the surface vector direction is lost. In the same way as 2D, the stepwise-smoothing process can improve the quality of the grid. The conflict detection method is applied to preventing overlap between adjacent grids in three-dimension. It also has two main problems that are the same as two-dimensional case. The first problem is to reduce the computational time by applying three dimensional specific Octree data structure to reduce excessive cross-examination time. Secondly, after applying the collision detection technique, the grids are created too close to each other. The grid shrinking method is applied to ensure the interval between the grids. This is different from two dimensional grid generation.

In three-dimension, the grid-shrinking method is applied to smooth the advancing steps of the adjacent grid points. The grid-shrinking method utilizes the Laplacian smoothing to reduce the difference of advancing steps between adjacent points. When the advancing steps of the adjacent grid are smoothed, the grid generated in a layer-gap region can have the improved quality of the grid.

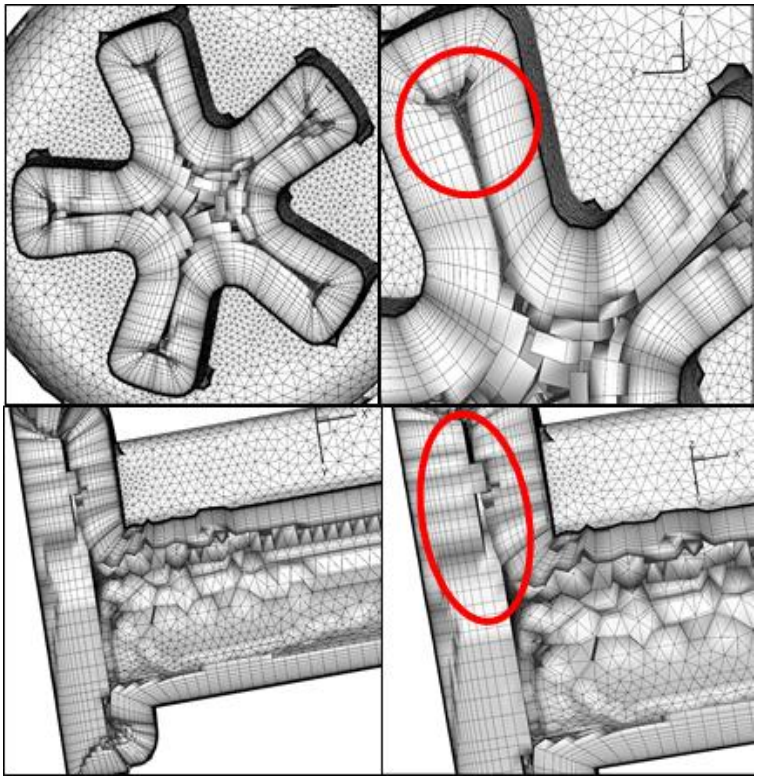

Fig. 21 Example of the application of the collision detection technique: 3D solid propellant shape (EBM) (top) Front cross-section (bottom) Side cross-section

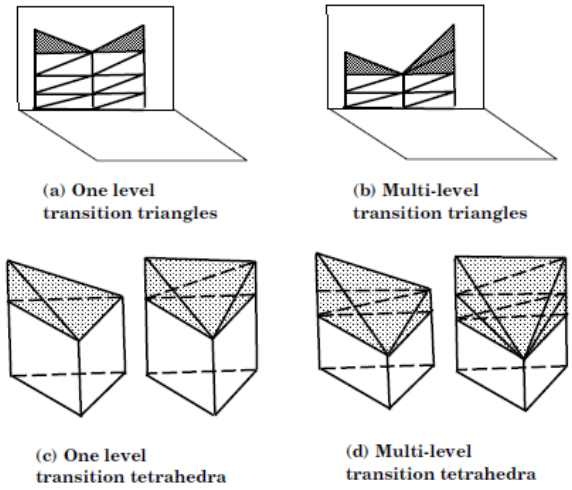

Fig. 22 Examples of the blending meshes [23]

In the gap between advancing steps of adjacent grid, the gap is filled with blending meshes. Blending meshes are designed to create pyramid grids if five grid points are needed and tetrahedral grids if four grid points are required. **Fig. 22** shows examples of blending meshes which are created to fill in difference of the grid advancing steps.

A simple test was conducted to confirm the applicability of the modified methods: grid shrinking method, skewness restriction. The test shape is a hexahedral shape that has 90 degrees of corners inside. A test was conducted to confirm the formation of the grid in relatively sharp areas.

Fig. 23 shows the gradually advancing procedure as modified methods accumulates. **(a)** is the generated grid that only applies the conflict-check procedure. In **(a)**, the meshes stack extremely close to other meshes. **(b)** is the generated grid that applies the conflict-check procedure and the grid shrinking method. It secures quite wider space than **(a)**. However, the meshes that have bad quality are made in the sharp region. **(c)** is the generated grid that applied conflict-check procedure, the grid shrinking method and the skewness restriction. The allowable skewness is limited by 0.7. . Compared to **(b),** the meshes that have bad quality is generally removed.

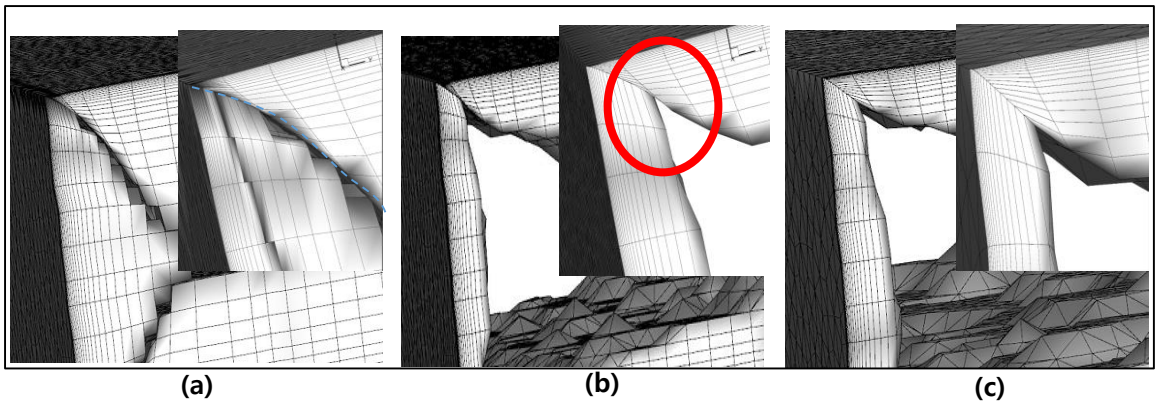

Fig. 23 Conflict test at the corner

(a) Conflict check only, (b) Shrinking method and (c) Skewness restriction

Another method is to apply the spring analogy for three dimension. This method has been used in the grid generation technique to improve the grid quality by widening the grid generation area. It is a method of finding the equilibrium grid connection assuming that adjacent grid points are connected to each other by tension springs. In order to test the elastic force between the two front planes, Eq. (13) is used to satisfy the following stop condition. When it is applied, an appropriate distance is secured between the faces coming parallel to each other.

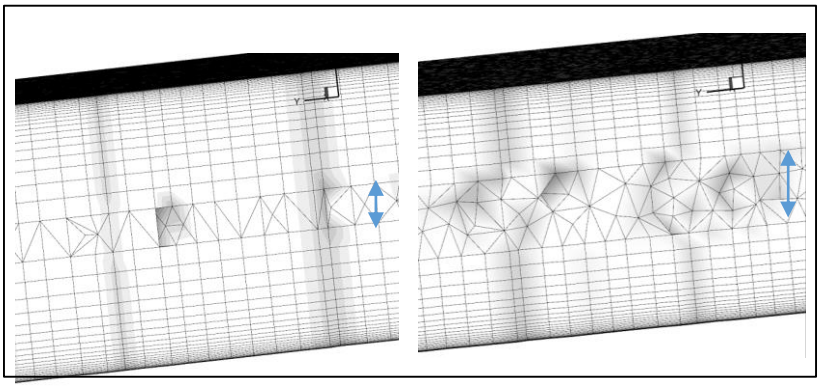

Fig. 24 Spring analogy application example 1:

(L) Before application, (R) After application

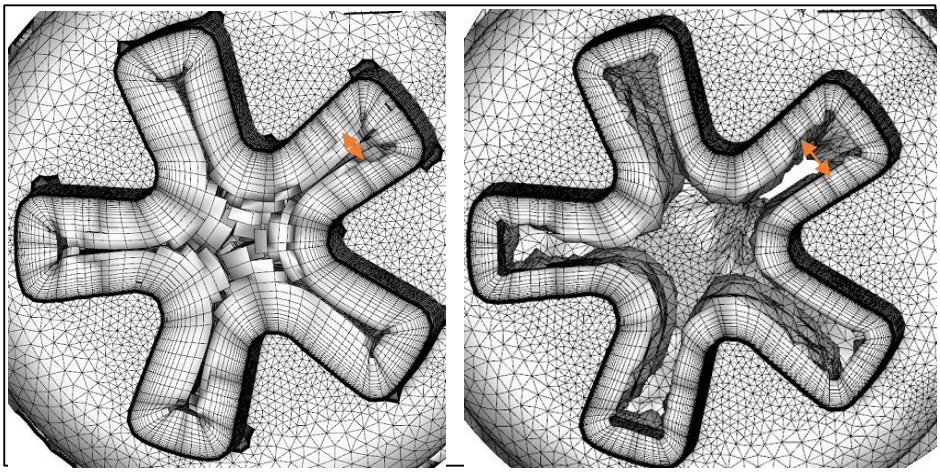

Fig. 25 Spring analogy application example 2:

(L) Before application, (R) After application

Grid generation is performed for three dimensional solid propulsion engine(EBM). The **Fig.26** is cross-sectional views of the generated grid. The upper one is a front section and the other is a cross section. Generate generation is performed until their cells are conflict or reach limited layer. Then grid shrinking method and spring analogy are performed to widen spacing between grids. In the remaining region, the tetrahedral grids are generated. Compared with the grid generated by Pointwise T-Rex. The grid generation are similar. The quality of the grid is shown in **Fig 27**.

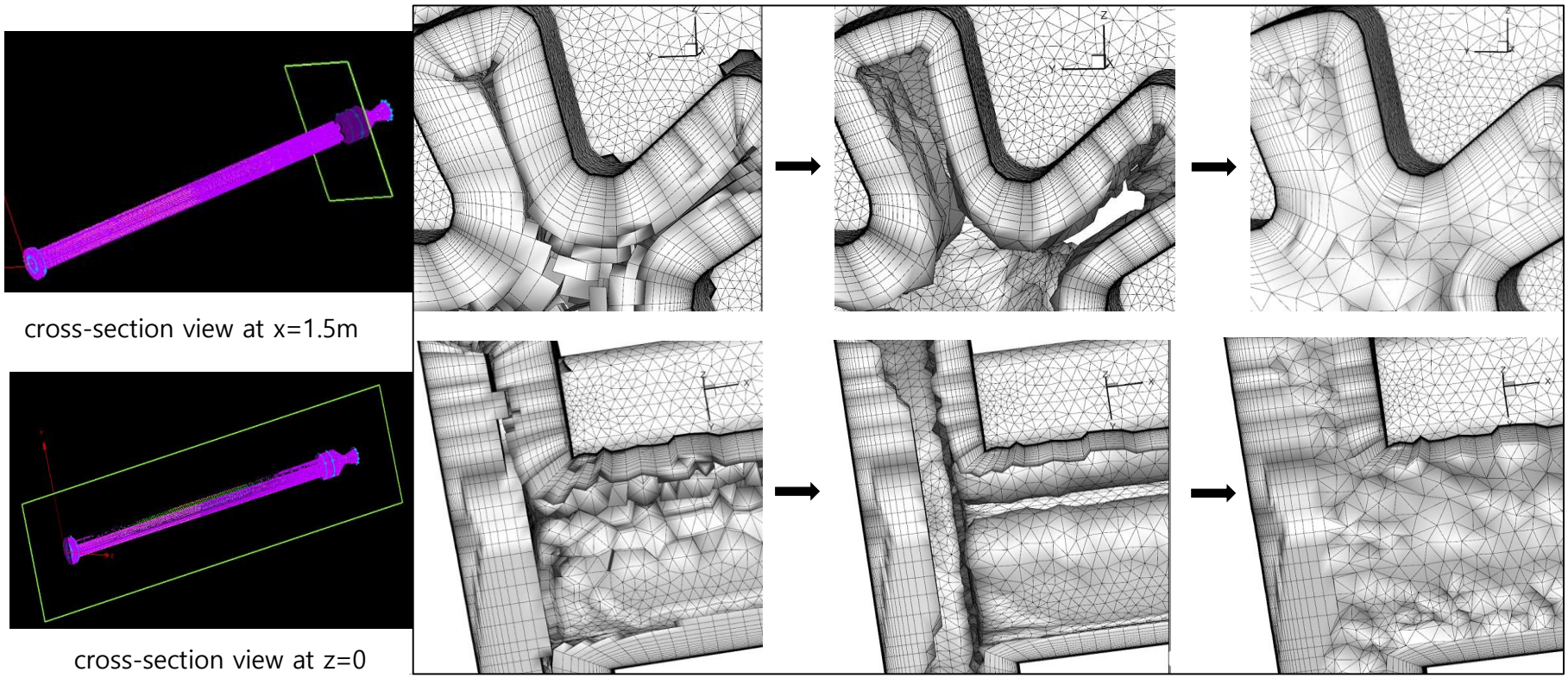

Fig. 26 Application example: 3-D solid propellant rocket motor configuration (EBM) (top) front-cross section (bottom) side-cross section

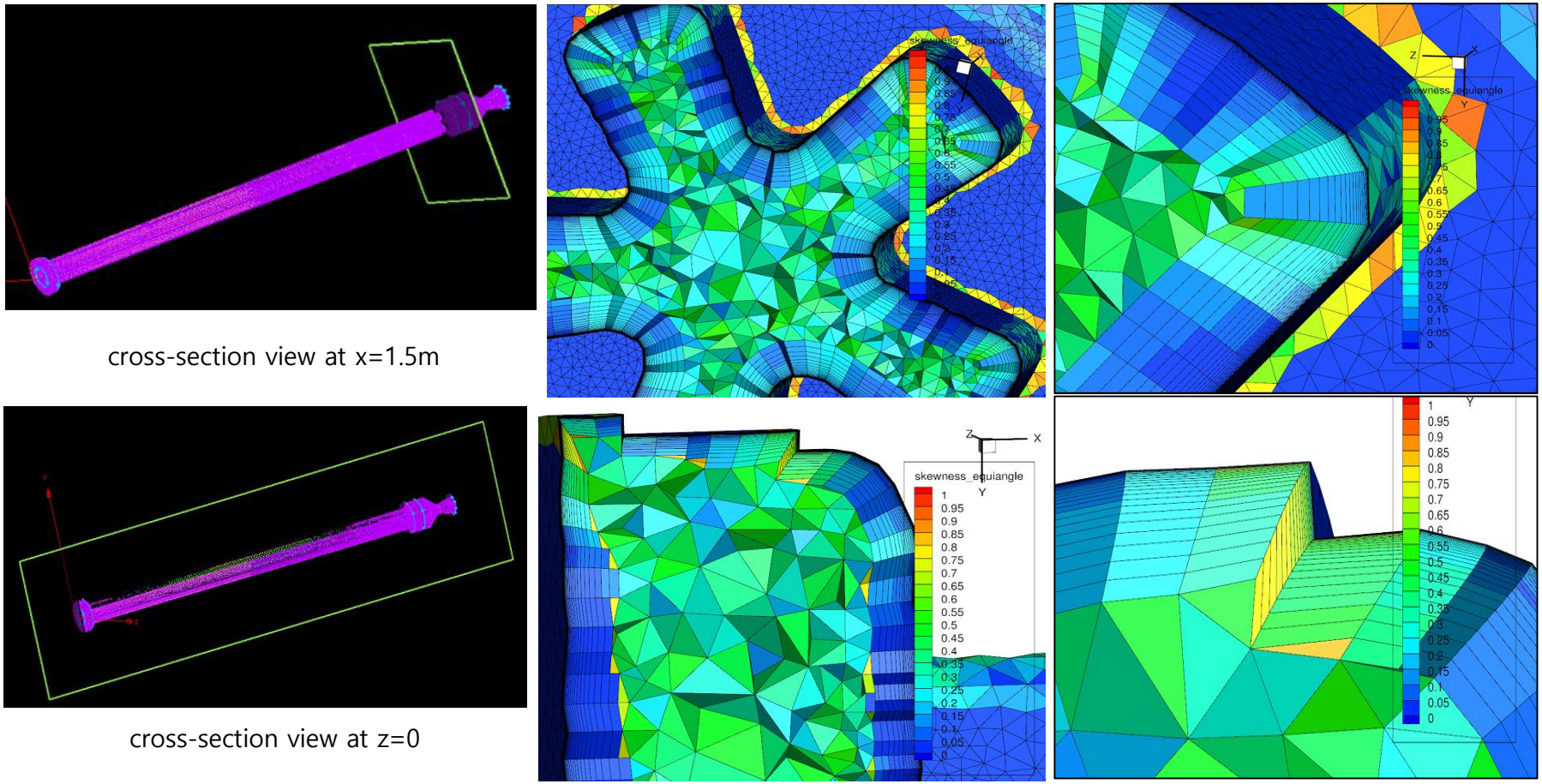

Fig. 27 Application example: 3D solid propellant rocket motor configuration (EBM) (top) front-cross section (bottom) side-cross section

The quality of the grid is compared with skewness and area ratio. The average grid quality on skewness, and area ratio is similar. However, when the skewness less than 0.1 is , This seems to be the reason for grid generation of the quality of the generation of a grid with a skewness of less than 0.5, rather than creating a quite great quality in Pointwise. Thus, the average of the skewness shows that quality of the code is better than Pointwise case.

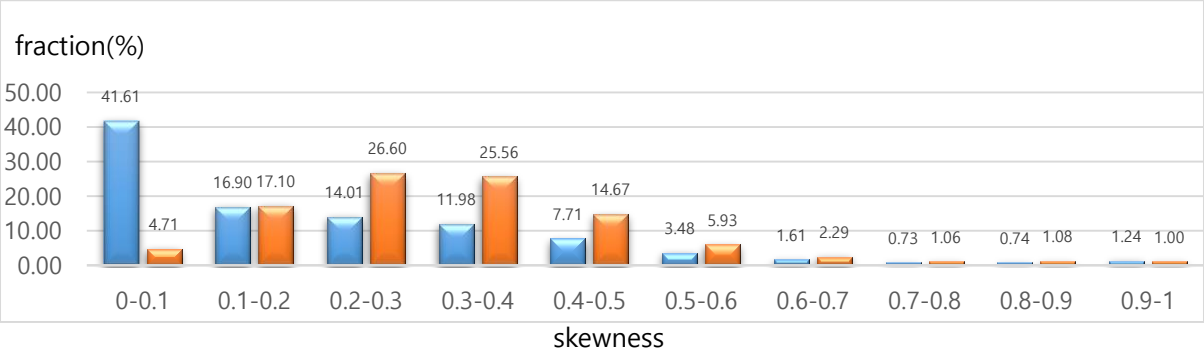

Fig. 28 Skewness histogram (blue) the code and (red) T-Rex

Table 7 Statistics of generated grids of the code and T-Rex

	code	T-Rex
The number of surface grid	79,212	79,212
The number of total grid	2,308,792	2,643,981
Skewness < 0.5 (%)	92.20	88.64
Skewness < 0.75 (%)	97.29	96.86
Skewness average	0.201	0.324
Area ratio < 0.5 (%)	99.02	98.78

Chapter 4

Grid regeneration program

The structure of the grid generation program is composed of a two-dimensional program and a three-dimensional program. The grid generation method consists of the internal flow grid generation method and the procedure of pre / post-processing for introducing the grid generation method. In addition, it includes the process of linking with the integration program for FSI.

4.1. Linking process with FSI solver

If the grid for the FSI solver program is poor quality, the grid generator can regenerate the grid through the regeneration module and transfer the necessary information to the solver.

The quality of the grid becomes worse as the flow region is deformed. If the quality of the grid used in the solver gets worse, the grid regeneration module starts to work. In order to maintain the grid quality, the regeneration procedure is performed and the information about the grid progress is obtained. Then the FSI analysis progresses using the newly created grid in the solver.

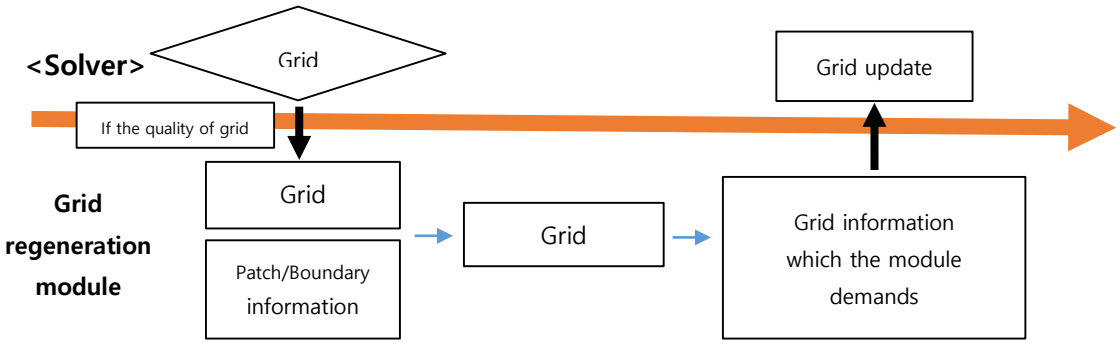

Fig. 29 Process interacting information between the FSI solver and the grid regeneration module

4.2. Overall procedure of grid regeneration module

The overall flow chart of the simulation is described in the **Fig. 30**. The entire grid generation process consists of the pre-processing procedure, the grid regeneration procedure, and the post-processing procedure.

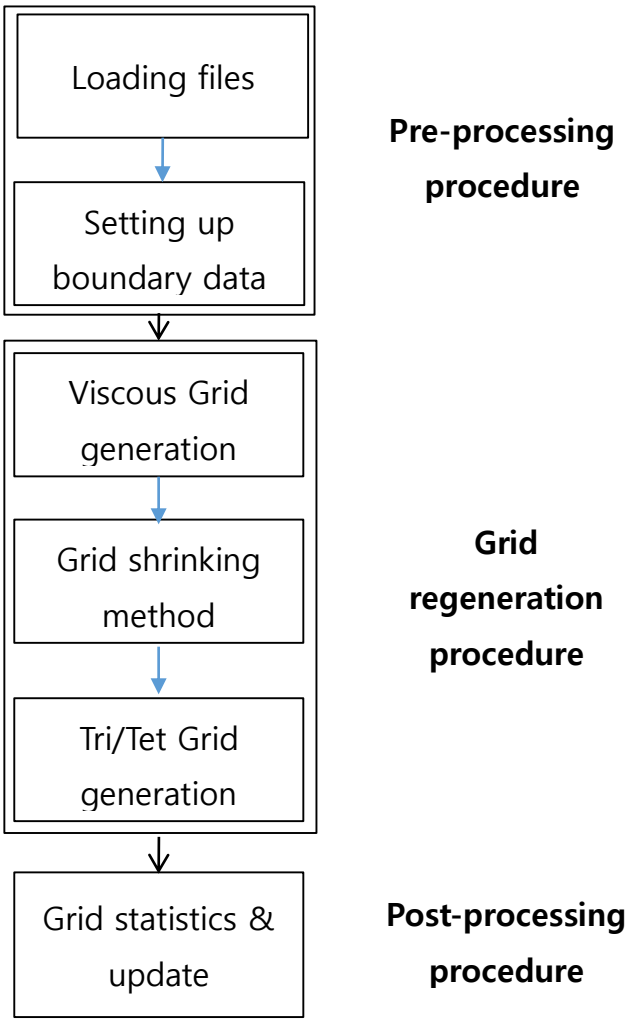

Fig. 30 Overall flow chart of the grid regeneration

1. Pre-processing procedure

Pre-processing process is the preparation process for creating the grid. After receiving the grid information from the solver, the grids are rearranged after grasping the surface grids connected. User-defined information (surface grid block which viscous grid generation occurs, grid block information) is matched for each grid. Information of the generated grid, and user-defined variable, grid generation, surface grid information is organized in data structure and automatically input them into the program. The detailed information is listed in **Table 8**.

Table 8 Surface grid information and user-defined information

Surface Grid Information	• Surface grid elements, coordinates • Patch/Boundary
User-defined variables	• Viscous grid generation area • Initial boundary layer thickness, growth rate • Smoothing function adjustment variable

2. Grid regeneration procedure

After pre-processing procedure, the grid regeneration process is performed in the grid generation process and generates the inner grid from the surface grid. The grid generation procedure consists of the regeneration of the viscous grid and creation of space to generate the unstructured grid.

The regeneration of the viscous grid: Viscous grid is generated using the grid generation technique for the internal flow. The entire viscous grid generation technique is applied and the following techniques are added to the Advancing-Layers Method as shown in **Fig.31.**

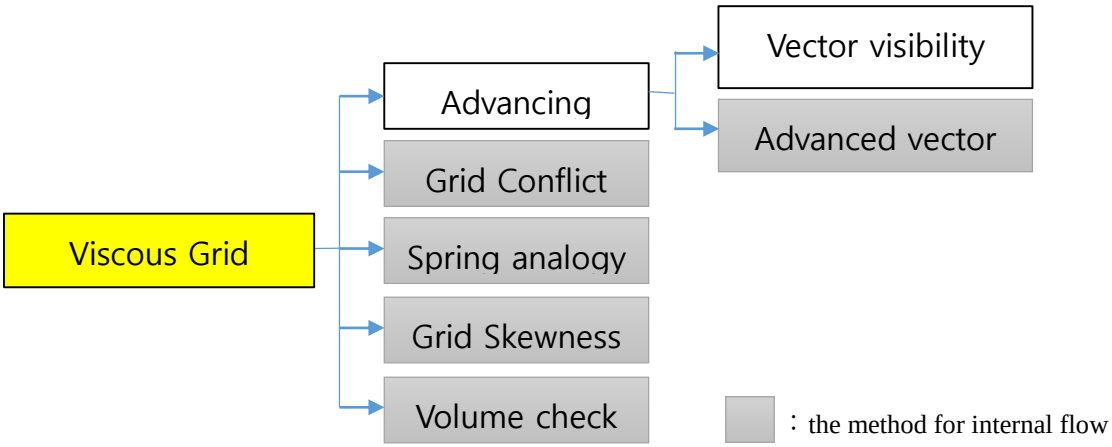

Fig. 31 Flow chart of the viscous grid generation

Creation of space to generate the unstructured grid: After creating the viscous grid, the poor quality meshes are eliminated through the grid shrinking method. Advancing step smoothing is a weighted Laplacian smoothing to alleviate the advancing layer-gap in the unstructured domain. Then, blending meshes are filled between layer-gap. Then a triangular / tetrahedral grid is generated in the remaining area.

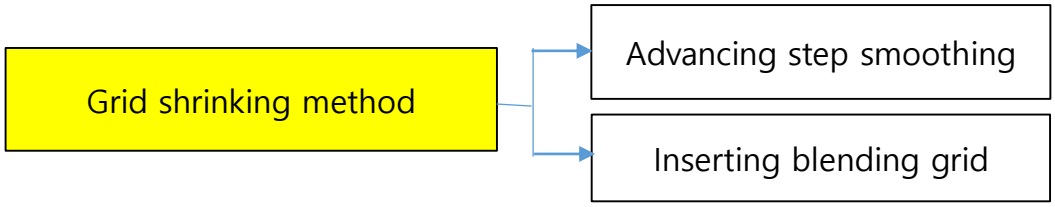

Fig. 32 Grid shrinking method

3. post-processing procedure

To transfer information of the generated grid to FSI solver, post-processing procedure is required. The generated grid information and surface information are sent to the integrated FSI solver.

Table 9 Information for the post-process procedure

Updated information of surface grid	• Grid elements, coordinates, edge/face/cell connections • Type of grid shape
Information of surface grid	• Surface grid elements, coordinates, edge/face connections. • Boundary information (ex. Case, Propellant, Outlet) • Patch information

The detailed techniques applied to the 2D and 3D grid generation modules of this regeneration program are summarized in **Table10**.

Table 10 Detailed techniques applied to the 2-D and 3-D grid generation modules

2-D	3-D
Advancing-layers Method -Smoothing method surface vectors, advancing vectors	Advancing-layers Method -Smoothing method surface vectors, advancing vectors - Vector Visibility condition
Conflict detecting method - Conflict check - Skewness restriction - Shrinking method	Conflict detecting method - Spring analogy - Skewness restriction - Conflict check -Bounding box - Shrinking method
Triangular mesh generation method - Bowyer/Watson algorithm	Tetrahedra mesh generation method - TetGen
Quad-Tree data structure	Octree data structure
Grid quality refinement	

Chapter 5

Applications

By using the grid generation module, the grids are generated for two-dimensional and three dimensional solid propellant rocket and other complex configurations. In 5.1, complicated surface models are selected to test the robustness of the program. In 5.2. the grids are generated for several types of solid-propellant rocket motors. The generated grids are used for the FSI analysis of the solid-propellant motor.

5.1. Applications on complex geometries

Before creating solid propellant grids, the grids for various complex configurations for testing purposes. The shapes if **Fig. 33** are opted for a representative test-configuration. In **table 11**, the statistics of the grids for three complex configurations: Human Brain, Spine and SAV. Because surface grids have sharp regions, the quality of the grid is decrease slightly. However, if the sharp region has more dense point distribution, the quality of the grid would be improved.

.

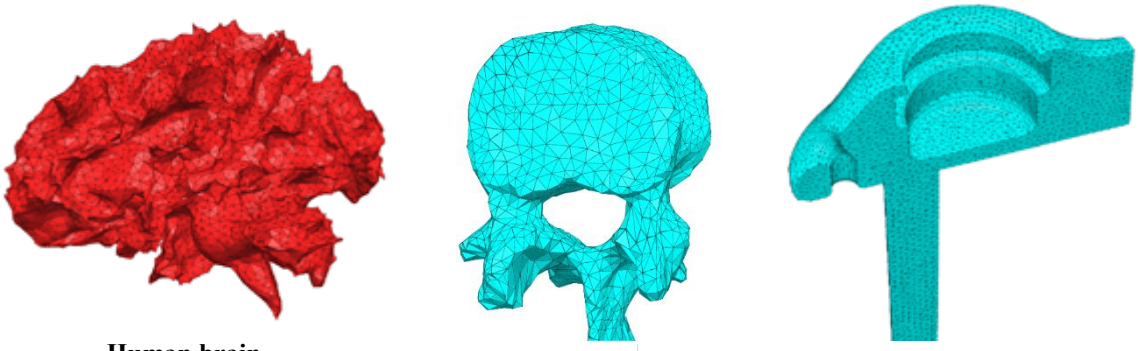

Fig. 33 Three point sets (scanned data sets from surfaces) used for experiments

Table 11 Statistics for generated grids of three test configurations

	Human brain	Spine	SAV
The number of surface nodes	10,477	1,932	6,788
The number of surface triangles	21,026	3,864	13,576
The number of total grid	708,107	5,786	488,288
Skewness < 0.5 (%)	73.78	80.23	87.94
Area rato < 5 (%)	90.26	92.56	96.84

5.2. Applications on solid-propellant rocket motors.

The grids for the internal flow region of the solid-propellant rocket motor are generated using the grid generation module. The flow profile and material property information of solid-propellant rocket motor are provided by ADD.

5.2.1 Two-dimensional Solid-propellant rocket motor

Second stage of Anti-Aircraft Missile (AAM) : Anti-Aircraft Missile, a solid propellant rocket used for intercepting airplanes is tested for grid generation. It is interpreted as a two-dimensional axisymmetric configuration, and it is set up to generate point in the area of contact with flow area, case, and propellant area. The initial BL spacing is set to $\mathbf{6.0 \times 10^{-6}}$. The number of surface edge is set to 1199, and the total number of generated grid is 41708. Maximum advancing step is set to 20. The number of NS grid is 25159, which is 60.3% of the total grid. The skewness histogram and the area ratio histogram are in **Fig 35**. The flow field analysis is performed using the generated grid.

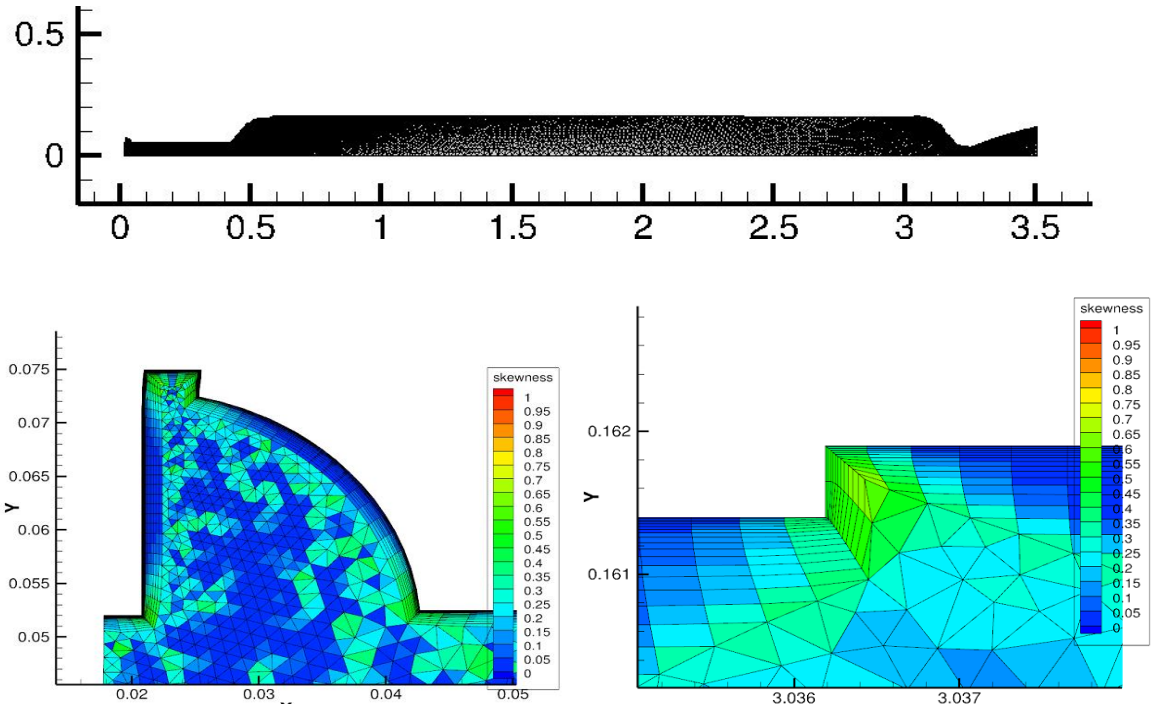

Fig. 34 skewness distribution of AAM second stage

Table 12 Statistics of the generated Grid of AAM

The number of the surface grid	**1,199**
The number of the total grid	**41,708**
Skewness < 0.5 (%)	**99.72**
Area ratio < 5 (%)	**98.17**

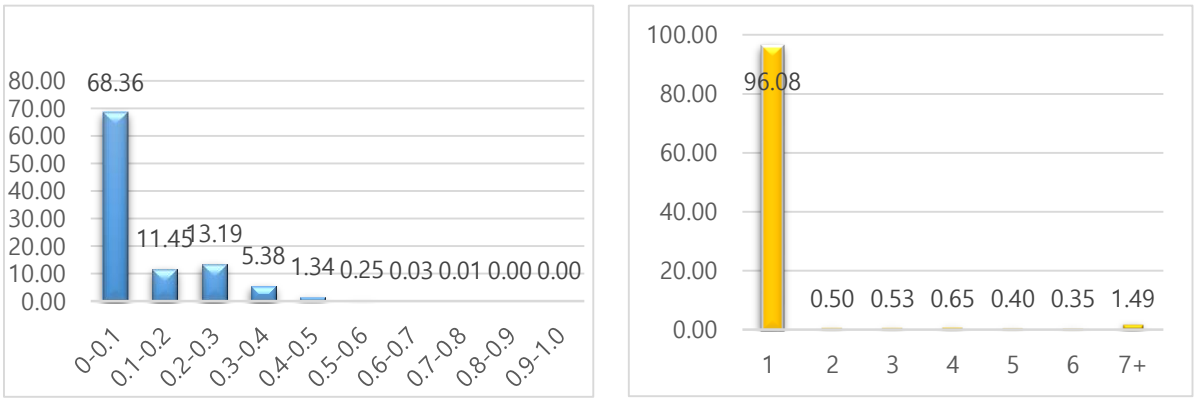

Fig. 35 Histogram of the generated grid (a) skewness, (b) Area ratio

The flow analysis is performed under the following conditions. Simulation algorithm of the solver utilizes TVDRK3 as the time integration method, AUSMPW + as the flux scheme, and Venkatakrishnan as the limiter. The simulation proceeds until the flow pressure converges to observe the phenomenon after the ignition. The unsteady flow analysis is performed until 1 second after ignition. **Fig. 34** is the result of regeneration with the grid created for AAM. The generated grid is used for analysis for 1 second after ignition. In **Fig. 36**, it converges to a constant state after 0.6 seconds. The internal pressure converges to approximately 2.6 Mpa. In **Fig. 37**, Using the generated grid of the AAM configuration, the flow that changes with time is analyzeed. This is a typical solid

rocket-shaped flow pattern. The initial short-time flow after ignition is intense but gradually converges.

Table 13 Algorithm settings for the FSI solver

Input information of the solver	
Mesh	Unstructured polygon
Time integration	TVDRK3
Flux scheme	AUSMPW+
Limiter	Venkatakrishnan

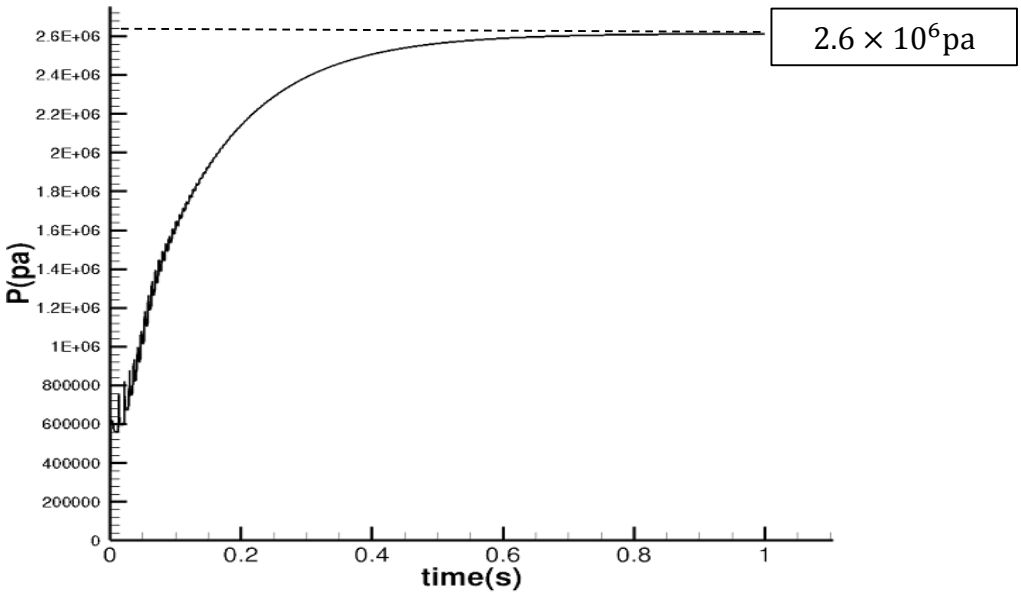

Fig. 36 Pressure profile at the AAM outlet

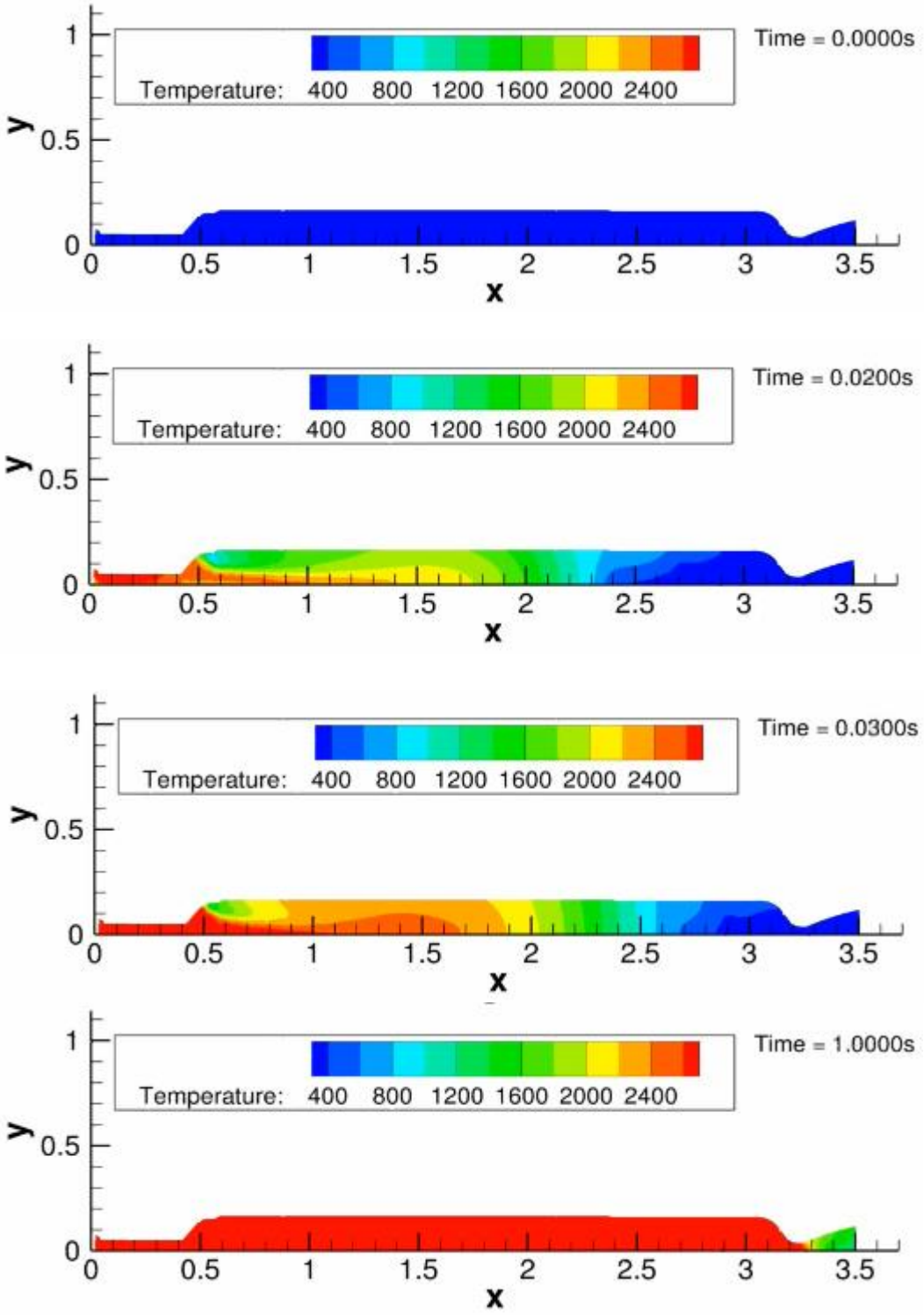

Fig. 37 Simulation results with time change (t=0.00s, 0.02s, 0.03s, 1.00s respectively)

Bore choke motor (EBM): The following model is a Bore Choke motor with the characteristic that the propellant region is pushed back when burned. **Fig 37** is the result of FSI analysis. Compared to the initial configuration, the propellant region is pushed backward significantly. **Fig. 38** shows a comparison of the shape before and after the change of shape.

FSI analysis on the generated grid is performed considering the viscous layer. In order to confirm whether the viscous grid is generated and analyzed for the case where the shape change is harsh.

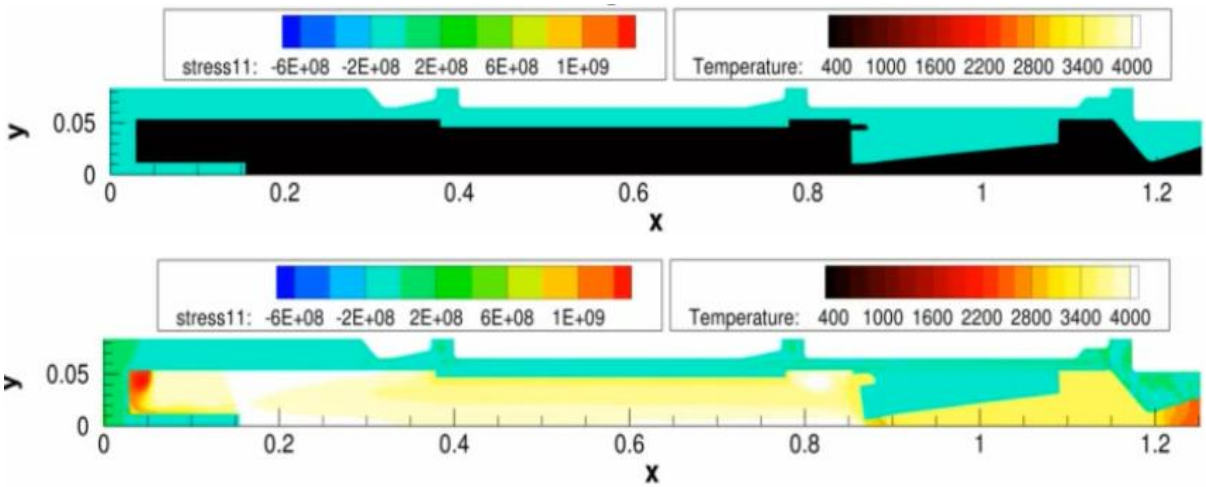

Fig. 38 temperature/stress contour before/after deformation

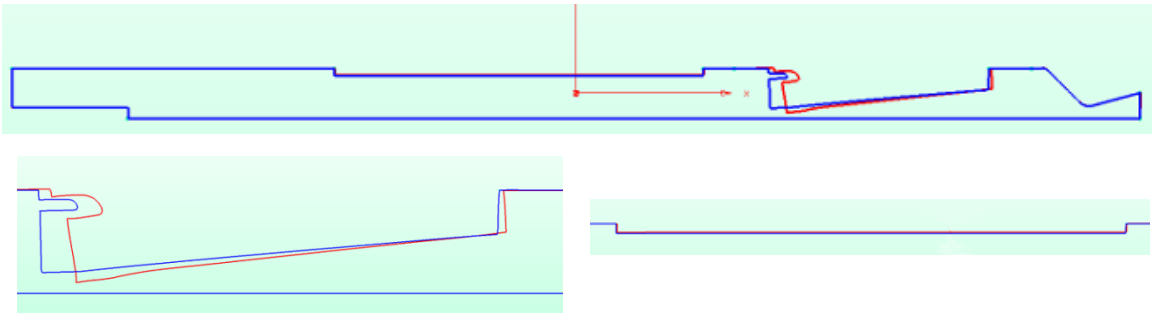

Fig. 39 Comparison with before/after conbustion of BCM

(Blue) Initial ignition and (Red) 0.824s after ignition

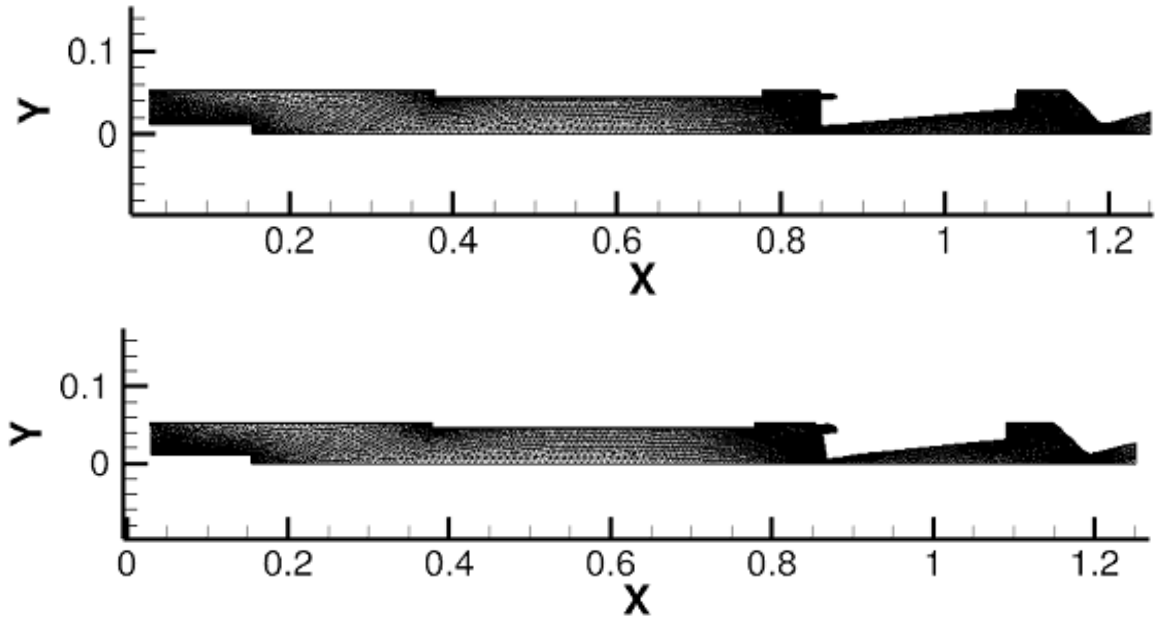

Fig. 40 Generated grid of BCM, (top) Initial ignition, (bottom) 0.824s after ignition

Table 14 information of the generated grid before/after deformation

	Before Deformation	**After Deformation**
The number of the surface grid	1136	1136
The number of the total grid	24921	25460
Skewness < 0.5 (%)	99.49	99.23
Area ratio < 5 (%)	99.18	99.22

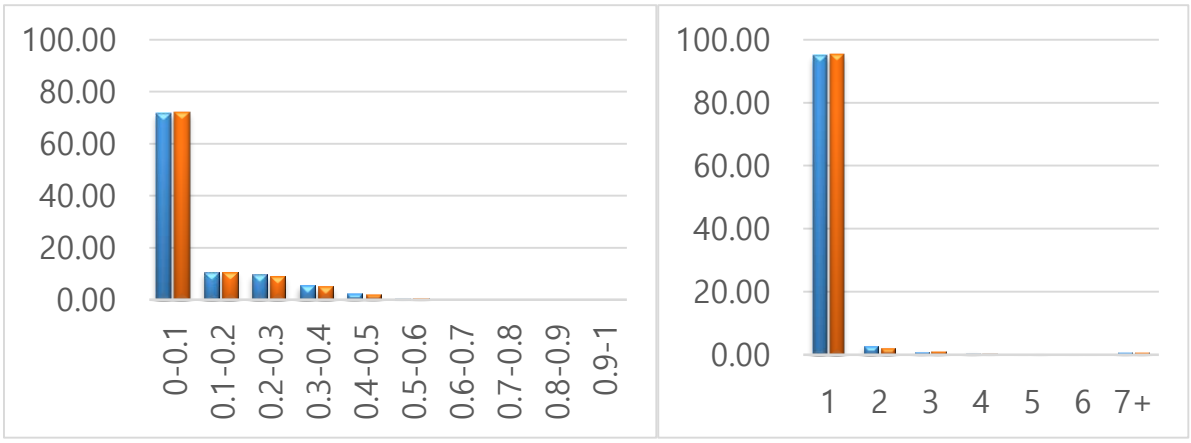

Fig. 41 Histogram of skewness and area ratio of BCM

The grid is generated and the quality of the grid is checked before and after deformation. The quality of the grid is checked in terms of skewness and area ratio in **Fig.40**. It can be seen that the grid is generated in this narrow region without failure. The flow analysis was performed for the BCM before the deformation and after the deformation respectively. It is confirmed that the flow analysis is physically explained. In addition, the boundary layer can be caught near boundary wall in **Fig. 42**.

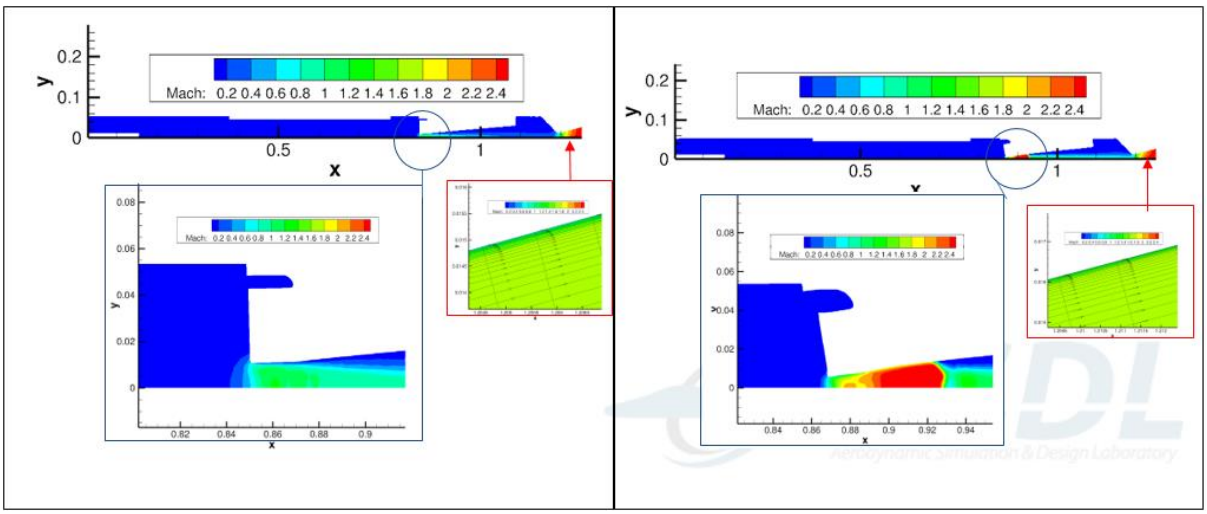

Fig. 42 Mach contour configuration and detection of boundary layer at (a) t=0s and (b) t= 0.824s

6.2.1 Three-dimensional Solid-propellant rocket motor

Erosive burning motor: The following model is an Erosive Burning Motor that has a three-dimensional configuration. The EBM model shown in **Fig 43**. In **Fig. 44**, as the combustion proceeds, the flow region gradually expands. Viscous grid is created before and after the combustion. At the generated grid,

In order to reduce the computational load and time, one-fifth (72^o) of the overall shape was analyzed. As the combustion proceeds, the propellant burns and the flow area expands. FSI analysis is performed until t = 0.234s after ignition.

Fig. 43 3-D configuration of Erosive Burning Motor

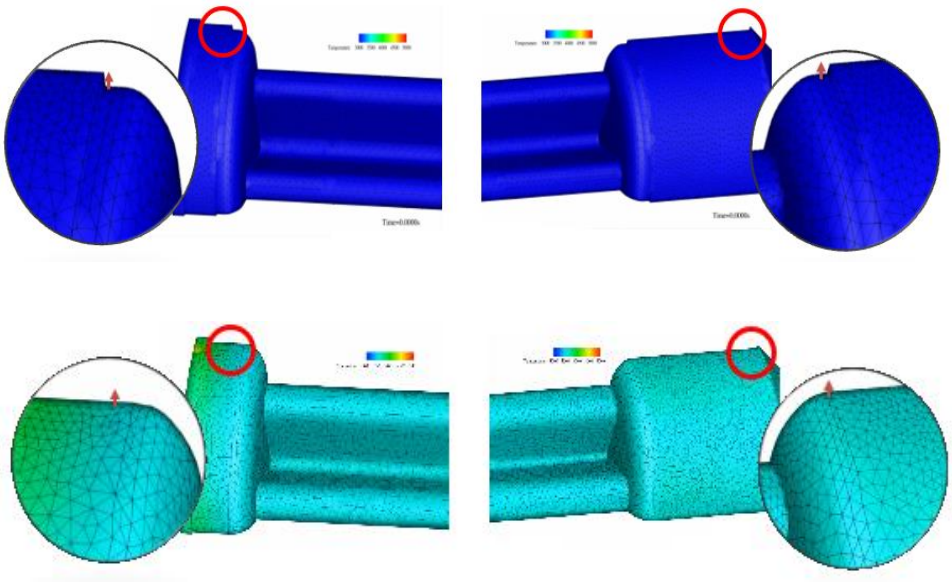

Fig. 44 Temperature contour of numerical simulation result.

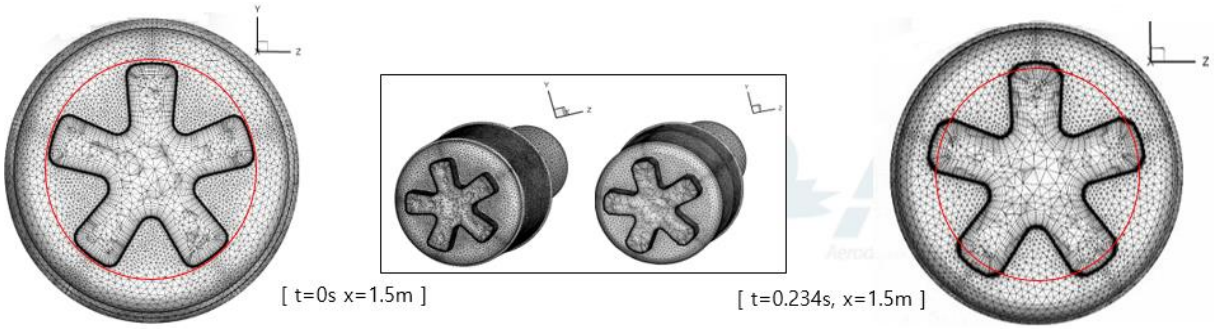

Fig. 45 Change in fluid domain (L) at t =0s, (R) at t = 0.234s

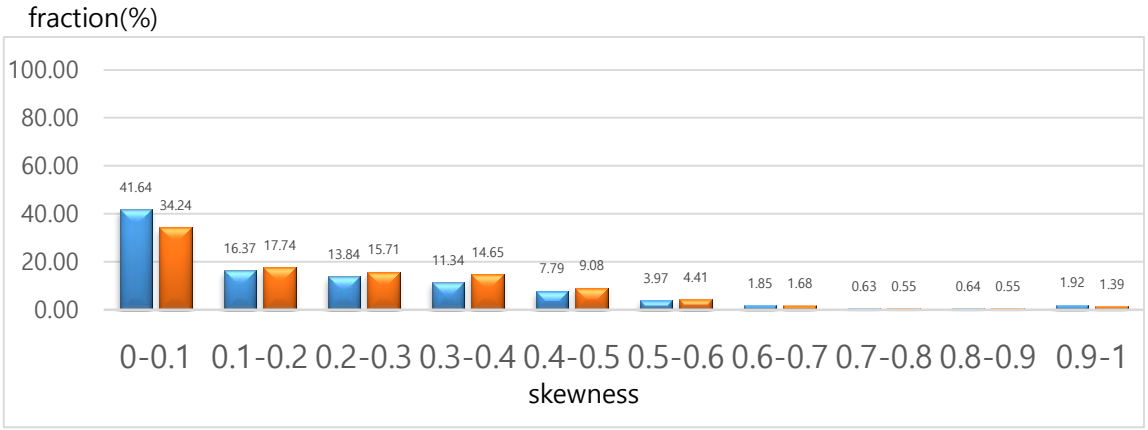

Fig. 46 Skewness histogram of EBM

The grids are generated configuration at t=0s, and t= 0.234s. Surfaces are obtained by FSI analysis. Both grids have a grid number of about 2 million. Both generated grids are compared as skewness and area ratio histogram in **Fig 46**. The flow analysis was performed for the BCM before the deformation and after the deformation respectively. It is confirmed that the flow analysis is physically explained. In addition, the boundary layer can be caught near boundary wall in **Fig. 47**.

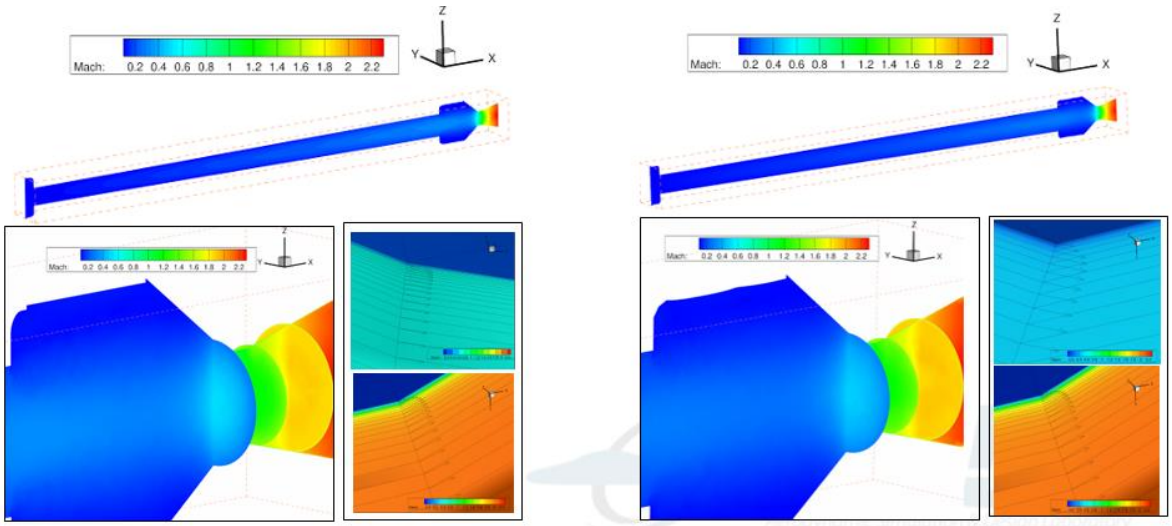

Fig. 47 Mach contour configuration and detection of boundary layer at (a) t=0s and (b) t= 0.234s

Chapter 6

Conclusion

In the case of the solid-propellant motor, the inside of the motor continuously changes with the combustion of the propellant. The grid generation technique for deforming region in the combustion surface is needed. In order to analyze the flow inside the combustion chamber of the solid propellant rocket motor, it should be considered for deforming region of combustion chamber. For this reason, automatic generation process of the unstructured-viscous grid is required for the FSI analysis. Prior works in grid generation has mainly focused on external flow for the viscous grid generation. Although the conventional method has advantages on the flexibility and generality of the grid generation, the method has limitation on internal flow for grid-overlap and conflict each other.

In this paper, the problems of the grid generation of the combustion chamber of the solid-propellant rocket motors are introduced and an overview of the methods and techniques used by the grid regeneration module is presented. In order to create the grid suitable for internal flow, the grid generation module is developed to efficiently generate a grid suitable for internal flow by adding several methods for the internal flow. The grid shrinking method and skewness restriction are applied to improve the quality of the grid and prevent the viscous grid from overlapping and proximity. As a result, the grid by using modified methods is generated maintaining the quality of the grid in complicated configurations. It is confirmed that the quality of the grid is maintained at a certain level analyzed in terms of the skewness and the area ratio.

Two-dimensional and Three-dimensional grid regeneration module have been developed and add introduced methods for applying complex internal flow geometry. Grids for two and three dimensional configuration are generated and analyzed for solid-propellant rocket motors and various shapes. The grid regeneration module is connected to the FSI integration program and the flow analysis is performed on the two- and three-dimensional solid-propellant rocket motor. In the grid

analysis, it is confirmed that the boundary layer is captured and analyzed, and it can be applied to the other continuously deforming configurations.

In the future, the grid generation module has plans to apply and analyze various shapes of solid propellant rocket motor with the applicable grid quality improvement techniques and the FSI solver. In addition, a computational acceleration method will be needed in order to prepare for the analysis of the three-dimensional grid generation with high data usage.

Appendix A. Advancing-Layers Method by Pirzadeh [19,21]

The specification of the stretching vector in the anisotropic Delaunay triangulation is quite involved for geometrically complex domains. Therefore, the so-called advancing layers method proposed by Pirzadeh is more widely utilized. It can also be considered as a modified advancing-front technique.

The generation of stretched triangular (tetrahedral) grids by the advancing-layers

The Advancing-Layers Method proceeds according to the following steps.

Table 15 Advancing-Layers Method by Prizadeh

General steps of the Advancing-Layers Method
1. All of the boundary surfaces are triangulate. 2. Normal vectors at the boundary nodes are approximately computed. 3. Grid points along the surface normal are placed and layers of quadrilateral (prismatic in 3D) elements of increasing thickness are formed. 4. Growing each stack of elements until the front intersects either itself or another front, or until the cell aspect ratio becomes close to unity is continued.

The rest of the flow domain is then filled with isotropic tetrahedron. Usually the advancing-front methodology is employed, which starts from the surface represented by the last layer of boundary cells.

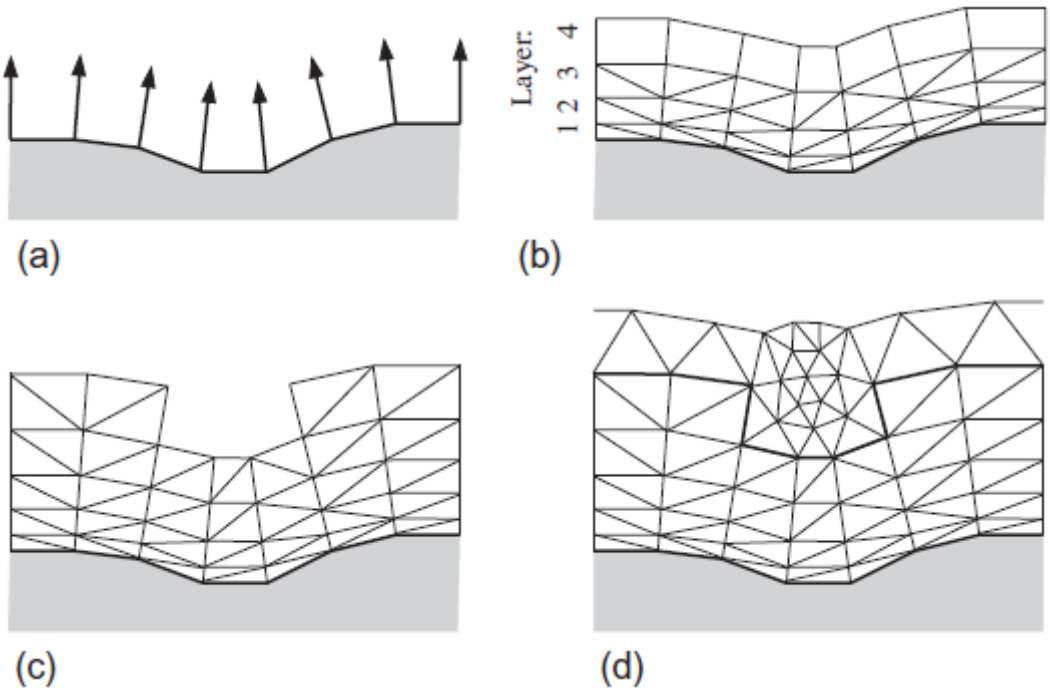

Fig. 47 Steps of the advancing-layer method: (a) computation of boundary normals, (b) generation of a new layer and subdivision of the elements, (c) finished stretched grid, (d) generation of isotropic elements in the rest of the domain

Appendix B. Skewness and Area/Volume ratio [24]

1. Skewness

Skewness means the degree of distortion of the shape of the cell. According to the definition of skewness, a value of 0 indicates an equilateral cell (best) and a value of 1 indicates a completely degenerate cell (worst). Degenerate cells (slivers) are characterized by nodes that are nearly coplanar (colinear in 2D). Highly skewed faces and cells are unacceptable because the equations being solved assume that the cells are relatively equilateral/equiangular. skewness is defined (in general) as

$$\mathbf{Skewness} = \mathbf{max}\left[\frac{\boldsymbol{\theta_{max}} - \boldsymbol{\theta_e}}{\mathbf{180} - \boldsymbol{\theta_e}}, \quad \frac{\boldsymbol{\theta_e} - \boldsymbol{\theta_{min}}}{\boldsymbol{\theta_e}}\right] \tag{14}$$

where θ_{max} is the largest angle in the face or cell, θ_{min}= smallest angle in the face or cell and θ_e= angle for an equiangular face/cell (e.g., 60 for a triangle, 90 for a square). For a pyramid, the cell skewness will be the maximum skewness computed for any face. An ideal pyramid (skewness = 0) is one in which the 4 triangular faces are equilateral (and equiangular) and the quadrilateral base face is a square.

2. Area/volume ratio

The area/volume ratio represents the uniformity of the size of the adjacent grids. The area ratio is called in two dimension and the volume ratio is called in three-dimension. The expression of area/volume ratio is shown as

$$\mathbf{Area/volume\ \ Ratio} = \mathbf{max}\left(\frac{\mathbf{Area_{cell}}}{\mathbf{min}\left(\mathbf{Area_{adjacent_{cell}}}\right)}, \frac{\mathbf{max}\left(\mathbf{Area_{adjacent_{cell}}}\right)}{\mathbf{Area_{cell}}} \right) \tag{15}$$

The Area/volume ratio functions are excellent diagnostics for finding cell size discontinuities at block and domain interfaces.

References

[1] P, George and O. Biblarz, Rocket Propulsion Elements, John Wiley & Sons, 9^{th} edition, 2011, 2016.

[2] D. Bošković and M. Krstić, “Stabilization of a solid propellant rocket instability by state feedback,” International Journal of Robust and Nonlinear Control, vol. 13, 2003, pp. 483, 495.

[3] W. A. Johnston, and J. W. Murdock, "Inside a Solid Rocket Motor During Ignition Transient," Jounal of Propulsion and Power vol.11, no.5, 1995, pp. 998,1005.

[4] S. Han and C. Kim. "Integrated Fluid–Structure Simulation for Full Burning of a Solid-Propellant Rocket Interior." Journal of Propulsional and Power, vol.30 no. 4., 2014.

[5] Hayri Yaman, Veli Çelik and Ercan Degirmenci, "Experimental investigation of the factors affecting the burning rate of solid rocket propellants," Journal of Fuel, vol. 115, 2013, p795.

[6] R. Fiedler, "Coupled Fluid-Structure 3-D Solid Rocket Motor Simulations." AIAA Journal. 2001-3954, 2001.

[7] S. Han, C. Kim and C. Lee, "A Full Burning FSI Simulation of Solid Propellant Rocket Interior," 50th AIAA Aerospace Sciences Meeting including the New Horizons Forum and Aerospace Exposition, Nashville, Tennessee, AIAA 2012-0038, 2012.

[8] J. Richard, T. Morel and F. Nicoud, "Effect of the Fluid-Structure Interaction on Solid Rocket Motors Instabilities," European Jounal of computional mechanics, vol. 21, pp. 337, 350.

[9] C. Farhat, "Provably second-order time-accurate loosely-coupled solution algorithms for transient nonlinear computational aeroelasticity." Computational Methods Application Mechanical Engineering, Vol 195, 2006, pp 1973, 2001.

[10] Mavriplis,"Unstructured Grid Techniques." Annu. Rev. Fluid. Mech, vol. 29, pp 472, 514.

[11] D. Meagher (1980). "Octree Encoding: A New Technique for the Representation,

Manipulation and Display of Arbitrary 3-D Objects by Computer."

[12] Schachter et al, "Two Algorithms for Constructing a Delaunay Triangulation." International Journal of Computer and Information Sciences vol. 9, No.8. 1980, pp219, 241

[13] S. Rebay. "Efficient Unstructured Mesh Generation by Means of Delaunay Triangulation and Bowyer-Watson Algorithm." Journal of computional physics, vol. 106, 1993, pp 125,138.

[14] H, Samat, “The Quadtree and Related Hierarchical Data Structures,” Computing Surveys, vol. 16, no. 2, 1984, pp204, 205

[15] D. Meagher, "Octree Encoding: A New Technique for the Representation, Manipulation and Display of Arbitrary 3-D Objects by Computer," Technical Report IPL-TR-80-111, 1980, pp13, 16.

[16] M. Tomac and D. Eller, "Towards automated hybrid-prismatic mesh generation." 23rd International Meshing Roundtable, 2014, pp. 4,5.

[17] S. Pirzadeh, "Viscous unstructured three-dimensional grids by the advancing-layers method," 32nd Aerospace Sciences Meeting & Exhibit, Reno, NV, 1994.

[18] W. M. Chan, "Overset Structured Hyperbolic Grid Generation on Triangulated Surfaces." Journal AIAA 2000-2245, Denver, CO, 2000.

[19] J. Blazak. Computational Fluid Dynamics Principles and Applications. Elsevier Ltd, 3rd edition, 2005, pp281, 283.

[20] F. J. Blom, "Considerations on the spring analogy," International Journal for Numerical Methods in Fluids, vol. 32, pp. 647, 668.

[21] S. Pirzadeh, "Unstructured viscous grid generation by the advancing-layers method." AIAA Journal, vol. 32, no.8, 1994, pp. 1735, 1737.

[22] S. Hang, "TetGen, a Delaunay-Based Quality Tetrahedral Mesh Generator," ACM

Transactions on Mathematical Software, vol. 41, No. 2, Article 11, p, 201.

[23] R. V. Garimella and M.S. Shephard, “Boundary Layer Meshing for Viscous Flows in Complex Domains,” In 7th International Meshing Roundtable, 1998.

[24] Pointwise, “ Pointwise®: User Manual,” Release 17, Pointwise, Inc., Fort Worth, TX, 2015.

국 문 초 록

고체추진기관 내부는 추진체의 연소와 고온·고압의 유동, 추진체의 구조변형이 서로 영향을 주고받는 복잡한 물리현상을 포함하고 있어 수치적인 해석에 많은 어려움이 따른다. 해석영역은 유동영역과 구조 및 연소영역으로 나누어지며 시간경과에 따라 각 영역별 변동이 발생한다. 따라서 해석 영역이 변동하는 형상에 맞는 격자를 생성하여야 하며, 이와 더불어 효율적이고 정확한 점성유동해석을 위한 경계층에 적합한 격자생성이 필요하다.

공탄성 해석과 같이 격자의 변형이 주기적인 경우에는 격자 이동 기법 및 격자 변형기법이 이용되고 있다. 반면 고체추진기관은 지속적 연소로 인한 영역의 변동이 일어나므로, 앞서 말한 문제와는 달리 상기한 두 기법으로는 격자 생성이 어렵다. 따라서 해석 중간에 전체적인 격자를 자동적으로 재생성을 하여야 하는데 이를 격자 재생성기법이라 한다. 격자 재생성 기법은 대개 사용자의 개입 없이 안정적이고 효율적인 격자생성 과정을 가지는 것이 중요하다.

본 연구에서는 고체로켓 2차원, 3차원 형상에 대하여 격자를 자동으로 생성할 수 있는 자동 재생성 프로그램을 개발한다. 또한 고체추진기관 형상에 대하여 자동으로 격자를 생성하고 해석을 수행한다.

주요어 : 고체추진기관, 유동-구조 연성 해석, 점성 격자, 경계층, 격자 재생성 기법,
격자 전진 기법(ALM)

학번 : 2016-20732